
gDDIM: Generalized denoising diffusion implicit models

Qinsheng Zhang
Georgia Institute of Technology
qzhang419@gatech.edu

Molei Tao
Georgia Institute of Technology
mtao@gatech.edu

Yongxin Chen
Georgia Institute of Technology
yongchen@gatech.edu

Abstract

Our goal is to extend the denoising diffusion implicit model (DDIM) to general diffusion models (DMs). Instead of constructing a non-Markov noising process as in the original DDIM paper, we examine the mechanism of DDIM from a numerical perspective. We discover that the DDIM can be obtained by using some specific approximations of the score when solving the corresponding stochastic differential equation. We present an interpretation of the accelerating effects of DDIM that also explains the advantages of a deterministic sampling scheme over the stochastic one for fast sampling. Building on this insight, we extend DDIM to general DMs with a small but delicate modification in parameterizing the score network. When applied to the critically-damped Langevin diffusion model, a new type of diffusion model proposed recently by augmenting the diffusion process with velocity, our algorithm achieves an FID score of 2.28, on CIFAR10, with only 50 number of score function evaluations (NFEs) and an FID score of 2.87 with only 27 NFEs, better than all existing methods with the same NFEs. ¹

1 Introduction

Generative models based on diffusion models (DMs) have experienced rapid developments in the past few years and show competitive sample quality compared with generative adversarial networks (GANs) [4, 21, 22], competitive negative log likelihood compared with autoregressive models in various domains and tasks [32, 10]. Besides, DMs enjoy other merits such as stable and scalable training, insensitivity to hyperparameters, and mode-collapsing resiliency [32, 17]. However, slow and expensive sampling prevents DMs from further application in more complex and higher dimension tasks. Once trained, GANs only forward pass neural network once to generate samples, but the vanilla sampling method of DMs needs 1000 or even 4000 steps [17, 6, 30] to pull noise back to the data distribution, which means thousands of neural networks forward evaluations. Therefore, the generation process of DMs is several orders of magnitude slower than GANs.

How to speedup sampling of DMs has received significant attention. With the seminal work by Song et al. [30] on the connection between stochastic differential equations (SDEs) and diffusion models, several studies investigate acceleration via solving the corresponding SDEs more efficiently [8, 17, 33]. Recently, a remarkable work by Dockhorn et al. [5], *critically-damped Langevin diffusion (CLD)*, proposes a velocity-augmented diffusion process and shows improved denoising efficiency. Most methods along this line still need hundreds of steps to generate high fidelity samples. Another

¹Code is available at <https://github.com/qsh-zh/gDDIM>

promising strategy is based on *probability flow* [30], which is an ordinary differential equations (ODE) associated with DMs that share equivalent marginal with SDE. Simple plug-in of off-the-shelf ODE solvers can already achieve significant acceleration comparing to SDEs-based methods [30, 5]. One of the arguably most popular sampling methods is *denoising diffusion implicit model (DDIM)* [28], which includes both deterministic and stochastic samplers, and both show tremendous improvement in sampling quality compared with previous methods when only a small number of steps is used for the generation. Deterministic DDIM in fact reduces to probability flow in the infinitesimal step size limit [28, 14]. Meanwhile, various approaches have been proposed to accelerate DDIM [13, 37, 14]. Recently, Zhang & Chen [42] discovered deterministic DDIM is an ODE numerical integrator based on exponential integrator, and employed exponential multistep method to further boost the efficiency of the ODE solver. (More related works in Appendix A.)

Although significant improvements of the DDIM in sampling efficiency have been observed empirically, the understanding of the mechanism of the DDIM is still lacking. First, why does solving probability flow ODE provide much higher sample quality than solving SDEs, when the number of steps is small? Second, it is shown that stochastic DDIM reduces to marginal-equivalent SDE [42], but its discretization scheme and mechanism of acceleration are still unclear. Finally, can we generalize DDIMs to other DMs and achieve similar or even better acceleration results?

In this work, we conduct a comprehensive study to answer the above questions, so that we can generalize and improve DDIM. We start with an interesting observation that the DDIM can solve corresponding SDEs/ODE **exactly** without any discretization error in finite or even one step, when the training dataset consists of only one data point. For deterministic DDIM, we find that the added noise in perturbed data along the diffusion is constant along an exact solution of probability flow ODE (see Prop 1). Besides, provided only one evaluation of log density gradient (a.k.a. score), we are already able to recover accurate score information for any datapoints, and this explains the acceleration of stochastic DDIM for SDEs (see Prop 3). Based on this observation, together with the manifold hypothesis, we present one possible interpretation to explain why the discretization scheme used in DDIMs is effective on realistic datasets (see Fig 2). Equipped with this new interpretation, we extend DDIM to general DMs, which we coin *generalized DDIM (gDDIM)*. With only a small but delicate change of the model parameterization, gDDIM can accelerate DMs based on general diffusion processes. Specifically, we verify the effectiveness of gDDIM on CLD.

To summarize, we have made the following contributions: 1) We provide an interpretation for the DDIM and unravel the mechanism of it. 2) The interpretation not only justifies the numerical discretization of DDIMs but also provides insights on why ODE-based samplers are preferred over SDE-based samplers when NFE is low. 3) We propose gDDIM, a generalized DDIM that can accelerate a large class of DMs. 4) We show by extensive experiments that gDDIM can drastically improve sampling quality/efficiency almost for free. Specifically, when applied to CLD, gDDIM can achieve an FID score of 2.87 with only 27 steps and 2.28 with 50 steps.

2 Background

In this section, we provide a brief introduction to diffusion models (DMs). Most DMs are built on two diffusion processes in continuous-time, one forward diffusion known as the noising process that drives any data distribution to a tractable distribution such as Gaussian by gradually adding noise to the data, and one backward diffusion known as the denoising process that sequentially removes noise from noised data to generate realistic samples. The continuous-time noising and denoising processes are modeled by stochastic differential equations (SDEs) [25].

In particular, the forward diffusion is a linear SDE with state $\mathbf{u}(t) \in \mathbb{R}^D$

$$d\mathbf{u} = \mathbf{F}_t \mathbf{u} dt + \mathbf{G}_t d\mathbf{w}, t \in [0, T] \quad (1)$$

where $\mathbf{F}_t, \mathbf{G}_t \in \mathbb{R}^{D \times D}$ represent the linear drift coefficient and diffusion coefficient respectively, and \mathbf{w} is a standard Wiener process. When the coefficients are piece-wise continuous, Eq (1) admits a unique solution [19]. Denote by $p_t(\mathbf{u})$ the distribution of the solutions $\{\mathbf{u}(t)\}_{0 \leq t \leq T}$ (simulated trajectories) to Eq (1) at time t , then p_0 is determined by the data distribution and p_T is a (approximate) Gaussian distribution. That is, the forward diffusion Eq (1) starts as a data sample and ends as a Gaussian random variable. This can be achieved with properly chosen coefficients $\mathbf{F}_t, \mathbf{G}_t$. Thanks to linearity of Eq (1), the transition probability $p_{st}(\mathbf{u}(t)|\mathbf{u}(s))$ from $\mathbf{u}(s)$ to $\mathbf{u}(t)$ is a Gaussian distribution. For convenience, denote $p_{0t}(\mathbf{u}(t)|\mathbf{u}(0))$ by $\mathcal{N}(\mu_t \mathbf{u}(0), \Sigma_t)$ where $\mu_t, \Sigma_t \in \mathbb{R}^{D \times D}$.

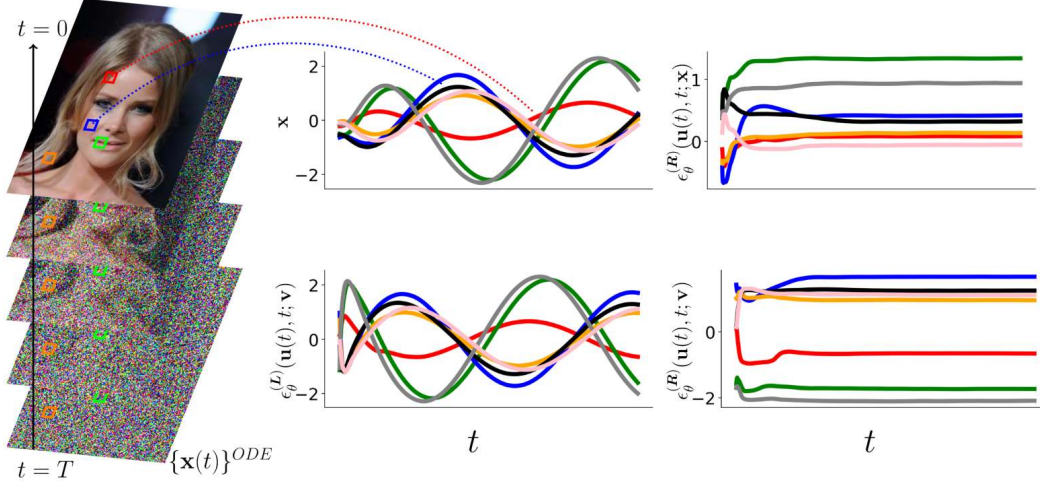


Figure 1: Importance of \mathbf{K}_t for score parameterization $\mathbf{s}_\theta(\mathbf{u}, t) = -\mathbf{K}_t^{-T} \epsilon_\theta(\mathbf{u}, t)$ and acceleration of diffusion sampling with probability flow ODE. Trajectory of probability ODE for CLD [5] and random pixel locations (Left). Pixel value and output of ϵ_θ in v channel with choice $\mathbf{K}_t = \mathbf{L}_t$ [5] along the trajectory (Mid). Output of ϵ_θ in x, v channels with choice $\mathbf{K}_t = \mathbf{R}_t$ (Right). The smooth network output enables large stepsize and thus sampling acceleration.

The backward process from $\mathbf{u}(T)$ to $\mathbf{u}(0)$ of Eq (1) is the denoising process. Remarkably, it can be characterized by the backward SDE simulated in reverse-time direction [31, 1]

$$d\mathbf{u} = [\mathbf{F}_t \mathbf{u} dt - \mathbf{G}_t \mathbf{G}_t^T \nabla \log p_t(\mathbf{u})] dt + \mathbf{G}_t d\mathbf{w}, \quad (2)$$

where \mathbf{w} denotes a standard Wiener process running backward in time. Here $\nabla \log p_t(\mathbf{u})$ is known as the score function. When Eq (2) is initialized with $\mathbf{u}(T) \sim p_T$, the distribution of the simulated trajectories coincides with that of the forward diffusion Eq (1). Thus, $\mathbf{u}(0)$ of these trajectories are unbiased samples from p_0 ; the backward diffusion Eq (2) is an ideal generative model.

In general, the score function $\nabla \log p_t(\mathbf{u})$ is not accessible. In diffusion-based generative models, a time-dependent network $\mathbf{s}_\theta(\mathbf{u}, t)$, known as the score network, is used to fit the score $\nabla \log p_t(\mathbf{u})$. One effective approach to train $\mathbf{s}_\theta(\mathbf{u}, t)$ is the denoising score matching (DSM) technique [31, 6, 36] that seeks to minimize the DSM loss

$$\mathbb{E}_{t \sim \mathcal{U}[0, T]} \mathbb{E}_{\mathbf{u}(0), \mathbf{u}(t) | \mathbf{u}(0)} [\|\nabla \log p_{0t}(\mathbf{u}(t) | \mathbf{u}(0)) - \mathbf{s}_\theta(\mathbf{u}(t), t)\|_{\Lambda_t}^2], \quad (3)$$

where $\mathcal{U}[0, T]$ represents the uniform distribution over the interval $[0, T]$. The time-dependent weight Λ_t is chosen to balance the trade-off between sample fidelity and data likelihood of learned generative model [32]. It is discovered in Ho et al. [6] that reparameterizing the score network by

$$\mathbf{s}_\theta(\mathbf{u}, t) = -\mathbf{K}_t^{-T} \epsilon_\theta(\mathbf{u}, t) \quad (4)$$

with $\mathbf{K}_t \mathbf{K}_t^T = \Sigma_t$ leads to better sampling quality. In this parameterization, the network tries to predict directly the noise added to perturb original data. Invoking the expression $\mathcal{N}(\mu_t \mathbf{u}(0), \Sigma_t)$ of $p_{0t}(\mathbf{u}(t) | \mathbf{u}(0))$, this parameterization results in the new DSM loss

$$\mathcal{L}(\theta) = \mathbb{E}_{t \sim \mathcal{U}[0, T]} \mathbb{E}_{\mathbf{u}(0) \sim p_0, \epsilon \sim \mathcal{N}(0, \mathbf{I}_D)} [\|\epsilon - \epsilon_\theta(\mu_t \mathbf{u}(0) + \mathbf{K}_t \epsilon, t)\|_{\mathbf{K}_t^{-1} \Lambda_t \mathbf{K}_t^{-T}}^2]. \quad (5)$$

Sampling: After the score network \mathbf{s}_θ is trained, one can generate samples via the backward SDE Eq (2) with a learned score, or the marginal equivalent SDE/ODE [30, 41, 42]

$$d\mathbf{u} = [\mathbf{F}_t \mathbf{u} - \frac{1 + \lambda^2}{2} \mathbf{G}_t \mathbf{G}_t^T \mathbf{s}_\theta(\mathbf{u}, t)] dt + \lambda \mathbf{G}_t d\mathbf{w}, \quad (6)$$

where $\lambda \geq 0$ is a free parameter. Regardless of the value of λ , the exact solutions to Eq (6) produce unbiased samples from $p_0(\mathbf{u})$ if $\mathbf{s}_\theta(\mathbf{u}, t) = \nabla \log p_t(\mathbf{u})$ for all t, \mathbf{u} . When $\lambda = 1$, Eq (6) reduces to reverse-time diffusion in Eq (2). When $\lambda = 0$, Eq (6) is known as the *probability flow ODE* [30]

$$d\mathbf{u} = [\mathbf{F}_t \mathbf{u} - \frac{1}{2} \mathbf{G}_t \mathbf{G}_t^T \mathbf{s}_\theta(\mathbf{u}, t)] dt. \quad (7)$$

DDPM and DDIM: A popular DM is the *Denoising diffusion probabilistic modeling (DDPM)* [6]. For a given data distribution $p_{\text{data}}(\mathbf{x})$, DDPM has state $\mathbf{u} = \mathbf{x} \in \mathbb{R}^d$ and sets $p_0(\mathbf{u}) = p_{\text{data}}(\mathbf{x})$. Though originally proposed in the discrete time setting, DDPM can be viewed as a discretization of a continuous-time SDE with parameters

$$\mathbf{F}_t = \frac{1}{2} \frac{d \log \alpha_t}{dt} \mathbf{I}_d, \quad \mathbf{G}_t = \sqrt{-\frac{d \log \alpha_t}{dt}} \mathbf{I}_d \quad (8)$$

for a decreasing scalar function α_t satisfying $\alpha_0 = 1, \alpha_T = 0$.

The sampling scheme proposed in DDPM is inefficient; it requires hundreds or even thousands of steps, and thus number of score function evaluations (NFEs), to generate realistic samples. A more efficient alternative is the *Denoising diffusion implicit modeling (DDIM)* proposed in Song et al. [28]. It has a similar training loss Eq (5) as DDPM but a different sampling scheme

$$\mathbf{x}(t_{i-1}) = \sqrt{\frac{\alpha_{t_{i-1}}}{\alpha_{t_i}}} \mathbf{x}(t_i) + (\sqrt{1 - \alpha_{t_{i-1}} - \sigma_{t_i}^2} - \sqrt{1 - \alpha_{t_i}}) \sqrt{\frac{\alpha_{t_{i-1}}}{\alpha_{t_i}}} \epsilon_\theta(\mathbf{x}(t_i), t_i) + \sigma_{t_i} \epsilon, \quad (9)$$

where $\{\sigma_{t_i}\}$ are hyperparameters and $\epsilon \sim \mathcal{N}(0, \mathbf{I}_d)$. DDIM can generate reasonable samples within 50 NFEs. For the special case where $\sigma_{t_i} = 0$, it is recently discovered in Zhang & Chen [42] that Eq (9) coincides with the numerical solution to Eq (7) using an advanced discretization scheme known as the *exponential integrator (EI)* that utilizes the semi-linear structure of Eq (7).

CLD: In Dockhorn et al. [5] the authors propose *critically-damped Langevin diffusion (CLD)*, a DM based on an augmented diffusion with an auxiliary velocity term. More specifically, the state of the diffusion in CLD is of the form $\mathbf{u}(t) = [\mathbf{x}(t), \mathbf{v}(t)] \in \mathbb{R}^{2d}$ with velocity variable $\mathbf{v}(t) \in \mathbb{R}^d$. The CLD employs the forward diffusion Eq (1) with coefficients

$$\mathbf{F}_t := \begin{bmatrix} 0 & \beta M^{-1} \\ \beta & -\Gamma \beta M^{-1} \end{bmatrix} \otimes \mathbf{I}_d, \quad \mathbf{G}_t := \begin{bmatrix} 0 & 0 \\ 0 & -\Gamma \beta M^{-1} \end{bmatrix} \otimes \mathbf{I}_d. \quad (10)$$

Here $\Gamma > 0, \beta > 0, M > 0$ are hyperparameters. Compared with most other DMs such as DDPM that inject noise to the data state \mathbf{x} directly, the CLD introduces noise to the data state \mathbf{x} through the coupling between \mathbf{v} and \mathbf{x} as the noise only affects the velocity component \mathbf{v} directly. It is argued that this property improves the performance of DMs [5]. It is observed in Dockhorn et al. [5] that CLD has more efficient noising and denoising processes and can generate high-quality samples with less NFEs compared with DDPM. See Section 4.3 for more discussions on CLD.

3 Revisit DDIM: Gap between exact solution and numerical solution

The complexity of sampling from a DM is proportional to the NFEs used to numerically solve Eq (6). To establish a sampling algorithm with a small NFEs, we ask the bold question:

Can we generate samples accurately from a DM with finite steps if the score function is precise?

To gain some insights to this problem, we start with the simplest scenario where the training dataset consists of only one data point \mathbf{x}_0 . It turns out that accurate sampling from diffusion models on this toy example is not that easy, even if the exact score function is accessible. Most well-known numerical methods for Eq (6), such as Euler integrator and Runge Kutta (RK) for ODE, Euler-Maruyama (EM) for SDE, are accompanied by discretization error and cannot recover the single data point in the train set unless infinite number of steps are used. Indeed, in general, the exact solution to Eq (6) requires the score information along the entire continuous-time solution trajectory while any numerical method can only evaluate the score function finite times.

Surprisingly, as we show below, DDIMs can recover the single data point in this toy example in finite steps, in fact, in one step. We first consider the deterministic DDIM, that is, Eq (9) with $\sigma_{t_i} = 0$. In view of Eq (8), the score network Eq (4) is $s_\theta(\mathbf{u}, t) = -\frac{\epsilon_\theta(\mathbf{u}, t)}{\sqrt{1 - \alpha_t}}$. To differentiate between the learned score and the real score, denote the ground truth version of ϵ_θ by ϵ_{GT} . In our toy example, the following property holds for ϵ_{GT} .

Proposition 1. Assume $p_0(\mathbf{u})$ is a Dirac distribution. Let $\mathbf{u}(t)$ be an arbitrary solution to the probability flow ODE Eq (7) with coefficient Eq (8) and the ground truth score, then $\epsilon_{\text{GT}}(\mathbf{u}(t), t) = -\sqrt{1 - \alpha_t} \nabla \log p_t(\mathbf{u}(t))$ remains constant along $\mathbf{u}(t)$.

We remark that even though $\epsilon_{\text{GT}}(\mathbf{u}(t), t)$ remains constant along an exact solution, the score $\nabla \log p_t(\mathbf{u}(t))$ is time varying. This underscores the advantage of the parameterization ϵ_θ over s_θ . Inspired by [Prop 1](#), we devise a sampling algorithm as follows that can recover the exact data point in one step for our toy example. This algorithm turns out to coincide with the deterministic DDIM.

Proposition 2. *With the parameterization $s_\theta(\mathbf{u}, \tau) = -\frac{\epsilon_\theta(\mathbf{u}, \tau)}{\sqrt{1-\alpha_\tau}}$ and the approximation $\epsilon_\theta(\mathbf{u}, \tau) \approx \epsilon_\theta(\mathbf{u}(t), t)$ for $\tau \in [t - \Delta t, t]$, the solution to the probability flow ODE [Eq \(7\)](#) with coefficient [Eq \(8\)](#) is*

$$\mathbf{u}(t - \Delta t) = \sqrt{\frac{\alpha_{t-\Delta t}}{\alpha_t}} \mathbf{u}(t) + (\sqrt{1 - \alpha_{t-\Delta t}} - \sqrt{1 - \alpha_t}) \sqrt{\frac{\alpha_{t-\Delta t}}{\alpha_t}} \epsilon_\theta(\mathbf{u}(t), t), \quad (11)$$

which coincides with deterministic DDIM.

When $\epsilon_\theta = \epsilon_{\text{GT}}$ as is the case in our toy example, there is no approximation error in [Prop 2](#) and [Eq \(11\)](#) is precise. This implies that deterministic DDIM can recover the training data in one step in our example. The update [Eq \(11\)](#) corresponds to a numerical method known as the exponential integrator to the probability flow ODE [Eq \(7\)](#) with coefficient [Eq \(8\)](#) and parameterization $s_\theta(\mathbf{u}, \tau) = -\frac{\epsilon_\theta(\mathbf{u}, \tau)}{\sqrt{1-\alpha_\tau}}$. This strategy is used and developed recently in Zhang & Chen [42]. [Prop 1](#) provides the sights on why such a strategy should work.

The above discussions however do not hold for stochastic cases where $\lambda > 0$ in [Eq \(6\)](#) and $\sigma_{t_i} > 0$ in [Eq \(9\)](#). Since the solutions to [Eq \(6\)](#) from $t = T$ to $t = 0$ are stochastic, neither $\nabla \log p_t(\mathbf{u})$ nor $\epsilon_{\text{GT}}(\mathbf{u}, t)$ remains constant over time; both are affected by the stochastic noise. The denoising SDE [Eq \(6\)](#) is more challenging compared with the probability ODE since it injects additional noise to $\mathbf{u}(t)$. The score information needs to remove not only noise presented in $\mathbf{u}(T)$ but also injected noise along the diffusion. In general, one evaluation of $\epsilon_\theta(\mathbf{u}, t)$ can only provide the information to remove noise in current state \mathbf{u} ; it cannot predict the injected noise. Can we do better? The answer is affirmative on our toy dataset. It turns out that $\nabla \log p_t(\mathbf{u}(t))$ along any stochastic trajectory $\{\mathbf{u}(t)\}$ is determined by $\nabla \log p_T(\mathbf{u}(T))$.

Proposition 3. *Assume SDE coefficients [Eq \(8\)](#) and that $p_0(\mathbf{u})$ is a Dirac distribution. Given any evaluation of the score function $\nabla \log p_s(\mathbf{u}(s))$, one can recover $\nabla \log p_t(\mathbf{u})$ for any t, \mathbf{u} as*

$$\nabla \log p_t(\mathbf{u}) = \frac{1 - \alpha_s}{1 - \alpha_t} \sqrt{\frac{\alpha_t}{\alpha_s}} \nabla \log p_s(\mathbf{u}(s)) - \frac{1}{1 - \alpha_t} (\mathbf{u} - \sqrt{\frac{\alpha_t}{\alpha_s}} \mathbf{u}(s)). \quad (12)$$

The major difference between [Prop 3](#) and [Prop 1](#) is that [Eq \(12\)](#) retains the dependence of the score over the state \mathbf{u} . This dependence is important in canceling the injected noise in the denoising SDE [Eq \(6\)](#). This approximation [Eq \(12\)](#) turns out to lead to a numerical scheme for [Eq \(6\)](#) that coincide with the stochastic DDIM.

Theorem 1. *Given the parameterization $s_\theta(\mathbf{u}, \tau) = -\frac{\epsilon_\theta(\mathbf{u}, \tau)}{\sqrt{1-\alpha_\tau}}$ and the approximation $s_\theta(\mathbf{u}, \tau) \approx \frac{1-\alpha_t}{1-\alpha_\tau} \sqrt{\frac{\alpha_\tau}{\alpha_t}} s_\theta(\mathbf{u}(t), t) - \frac{1}{1-\alpha_\tau} (\mathbf{u} - \sqrt{\frac{\alpha_\tau}{\alpha_t}} \mathbf{u}(t))$ for $\tau \in [t - \Delta t, t]$, the exact solution $\mathbf{u}(t - \Delta t)$ to [Eq \(6\)](#) with coefficient [Eq \(8\)](#) is*

$$\mathbf{u}(t - \Delta t) \sim \mathcal{N}\left(\sqrt{\frac{\alpha_{t-\Delta t}}{\alpha_t}} \mathbf{u}(t) + \left[-\sqrt{\frac{\alpha_{t-\Delta t}}{\alpha_t}} \sqrt{1 - \alpha_t} + \sqrt{1 - \alpha_{t-\Delta t} - \sigma_t^2}\right] \epsilon_\theta(\mathbf{u}(t), t), \sigma_t^2 \mathbf{I}_d\right) \quad (13)$$

with $\sigma_t = (1 - \alpha_{t-\Delta t}) \left[1 - \left(\frac{1 - \alpha_{t-\Delta t}}{1 - \alpha_t}\right)^{\lambda^2} \left(\frac{\alpha_t}{\alpha_{t-\Delta t}}\right)^{\lambda^2}\right]$, which is the same as the DDIM [Eq \(9\)](#).

Note that [Theorem 1](#) with $\lambda = 0$ agrees with [Prop 2](#); both reproduce the deterministic DDIM but with different derivations.

Dirac $p_0(\mathbf{u})$ and the manifold hypothesis: While [Prop 1](#) and [Prop 3](#) require the strong assumption that the data distribution is a Dirac, DDIMs work very effectively on realistic datasets, which may contain millions of datapoints [18]. Here we present one possible interpretation based on the manifold hypothesis [23].

It is believed that real-world data lie on low-dimensional manifold [34] embedded in a high-dimensional space and the data points are well separated in high-dimensional data space. For example, realistic images are scattered in pixel space and the distance between every two images

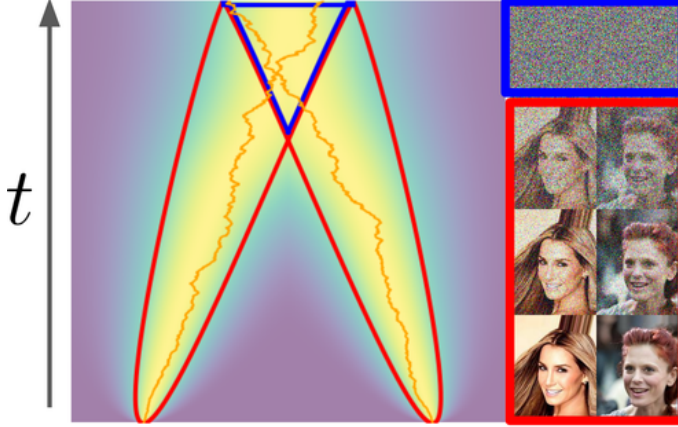


Figure 2: Manifold hypothesis and Dirac distribution assumption. We model images dataset as a mixture of well separated Dirac distribution and visualize diffusion process. Curves in **red** indicate high density area spanned by $p_{0t}(\mathbf{u}(t)|\mathbf{u}(0))$ by different mode and region surrounded by them indicates the phase when $p_t(\mathbf{u})$ is dominated by one mode while region surrounded by **blue** one is for the mixed phase. In the red region, we can approximate data score by score of dominated Dirac distribution. Such property can help accelerate sampling.

can be very large if measured in pixel difference even if they are similar perceptually. To model this property, we consider a dataset consisting of M datapoints $\{\mathbf{u}^{(m)}\}_{m=1}^M$. The exact score is

$$\nabla \log p_t(\mathbf{u}) = \sum_m w_m \nabla \log p_{0t}(\mathbf{u}|\mathbf{u}^{(m)}), \quad w_m = \frac{p_{0t}(\mathbf{u}|\mathbf{u}^{(m)})}{\sum_m p_{0t}(\mathbf{u}|\mathbf{u}^{(m)})},$$

which can be interpreted as a weighted sum of M score functions associated with Dirac distributions. This is illustrated in Fig 2. In the red color region where the weights $\{w_m\}$ are dominated by one specific data $\mathbf{u}^{(m^*)}$ and thus $\nabla \log p_t(\mathbf{u}) \approx \nabla \log p_{0t}(\mathbf{u}|\mathbf{u}^{(m^*)})$. The phenomenon caused by manifold hypothesis partially justifies the Dirac distribution assumption in Prop 1 and Prop 3, and explains the effectiveness of DDIMs.

4 Generalize and improve DDIM

The DDIM is specifically designed for DDPMs. Can we generalize it to other DMs? With the insights in Prop 1 and 3, it turns out that with a careful chosen \mathbf{K}_τ , we can generalize DDIMs to any DMs with general drift and diffusion. We coin the resulted algorithm the *Generalized DDIM* (gDDIM). Concretely, we apply the gDDIM to CLD to illustrate our approach.

4.1 Deterministic gDDIM with Prop 1

Toy dataset: Motivated by Prop 1, we ask whether there exists an ϵ_{GT} that remains constant along a solution to the probability flow ODE Eq (7). We start with a special case with data distribution $p_0(\mathbf{u}) = \mathcal{N}(\mathbf{u}_0, \Sigma_0)$. It turns out that any solution to Eq (7) is of the form

$$\mathbf{u}(t) = \Psi(t, 0)\mathbf{u}_0 + \mathbf{R}_t\epsilon \quad (14)$$

with a constant ϵ and a time-varying $\mathbf{R}_t \in \mathbb{R}^{D \times D}$ that satisfies $\mathbf{R}_0\mathbf{R}_0^T = \Sigma_0$ and

$$\frac{d\mathbf{R}_t}{dt} = (\mathbf{F}_t + \frac{1}{2}\mathbf{G}_t\mathbf{G}_t^T\Sigma_t^{-1})\mathbf{R}_t. \quad (15)$$

Here $\Psi(t, s)$ is the transition matrix associated with \mathbf{F}_τ ; it is the solution to $\frac{\partial \Psi(t, s)}{\partial t} = \mathbf{F}_t\Psi(t, s)$, $\Psi(s, s) = \mathbf{I}_D$. Interestingly, \mathbf{R}_t satisfies $\mathbf{R}_t\mathbf{R}_t^T = \Sigma_t$ like \mathbf{K}_t in Eq (4). Based on Eq (14) and Eq (15), we extend Prop 1 to more general DMs.

Proposition 4. Assume the data distribution $p_0(\mathbf{u})$ is $\mathcal{N}(\mathbf{u}_0, \Sigma_0)$. Let $\mathbf{u}(t)$ be an arbitrary solution to the probability flow ODE Eq (7) with the ground truth score, then $\epsilon_{\text{GT}}(\mathbf{u}(t), t) := -\mathbf{R}_t^T \nabla \log p_t(\mathbf{u}(t))$ remains constant along $\mathbf{u}(t)$.

A direct consequence of Prop 4 is that we can conduct accurate sampling in one step in the toy example since we can recover the score along any simulated trajectory given its value at $t = T$, if \mathbf{K}_t in Eq (4) is set to be \mathbf{R}_t . This choice $\mathbf{K}_t = \mathbf{R}_t$ will make a huge difference in sampling quality as we will show later. The fact provides guidance to design efficient sampling scheme for realistic data.

Realistic dataset: As the accurate score is not available for realistic dataset, we need to use learned score $s_\theta(\mathbf{u}, t)$ for sampling. With our new parameterization $\epsilon_\theta(\mathbf{u}, t) = -\mathbf{R}_t^T s_\theta(\mathbf{u}, t)$ and the approximation $\tilde{\epsilon}_\theta(\mathbf{u}, \tau) = \epsilon_\theta(\mathbf{u}(t), t)$ for $\tau \in [t - \Delta t, t]$, we reach the update step for deterministic gDDIM by solving probability flow with approximator $\tilde{\epsilon}_\theta(\mathbf{u}, \tau)$ exactly as

$$\mathbf{u}(t - \Delta t) = \Psi(t - \Delta t, t)\mathbf{u}(t) + \left[\int_t^{t-\Delta t} \frac{1}{2} \Psi(t - \Delta t, \tau) \mathbf{G}_\tau \mathbf{G}_\tau^T \mathbf{R}_\tau^{-T} \right] \epsilon_\theta(\mathbf{u}(t), t). \quad (16)$$

Multistep predictor-corrector for ODE: Inspired by Zhang & Chen [42], we further boost the sampling efficiency of gDDIM by combining Eq (16) with multistep methods [7, 42, 14]. We derive multistep *predictor-corrector* methods to reduce number of step while retaining accuracy [20, 26]. Empirically, we found that using more NFEs in predictor leads to better performance when the total NFE is small. Thus, we only present multistep predictor for deterministic gDDIM. We include the proof and multistep corrector in Appendix B. For time discretization grid $\{t_i\}_{i=0}^N$ where $t_0 = 0, t_N = T$, the q -th step predictor from t_i to t_{i+1} in term of ϵ_θ parameterization reads

$$\mathbf{u}(t_{i+1}) = \Psi(t_{i+1}, t_i)\mathbf{u}(t_i) + \sum_{j=0}^{q-1} [\mathbf{C}_{ij} \epsilon_\theta(\mathbf{u}(t_{i+j}), t_{i+j})], \quad (17a)$$

$$\mathbf{C}_{ij} = \int_{t_i}^{t_{i+1}} \frac{1}{2} \Psi(t_{i+1}, \tau) \mathbf{G}_\tau \mathbf{G}_\tau^T \mathbf{R}_\tau^{-T} \prod_{k \neq j} \left[\frac{\tau - t_{i+k}}{t_{i+j} - t_{i+k}} \right] d\tau. \quad (17b)$$

4.2 Stochastic gDDIM with Prop 3

Following the same spirits, we can generalize Prop 3

Proposition 5. Assume the data distribution $p_0(\mathbf{u})$ is $\mathcal{N}(\mathbf{u}_0, \Sigma_0)$. Given any evaluation of the score function $\nabla \log p_s(\mathbf{u}(s))$, one can recover $\nabla \log p_t(\mathbf{u})$ for any t, \mathbf{u} as

$$\nabla \log p_t(\mathbf{u}) = \Sigma_t^{-1} \Psi(t, s) \Sigma_s \nabla \log p_s(\mathbf{u}(s)) - \Sigma_t^{-1} [\mathbf{u} - \Psi(t, s)\mathbf{u}(s)]. \quad (18)$$

Prop 5 is not surprising; in our example, the score has closed form. Eq (18) provides an accurate score estimation for our toy dataset; it also serves as score approximator in realistic data.

Realistic dataset: Based on Eq (18), with the parameterization $s_\theta(\mathbf{u}, \tau) = -\mathbf{R}_\tau^{-T} \epsilon_\theta(\mathbf{u}, \tau)$, we propose the following gDDIM approximator $\tilde{s}_\theta(\mathbf{u}, \tau)$ for $\epsilon_\theta(\mathbf{u}, \tau)$

$$\tilde{\epsilon}_\theta(\mathbf{u}, \tau) = \mathbf{R}_\tau^{-1} \Psi(\tau, s) \mathbf{R}_s \epsilon_\theta(\mathbf{u}(s), s) + \mathbf{R}_\tau^{-1} [\mathbf{u} - \Psi(\tau, s)\mathbf{u}(s)]. \quad (19)$$

Proposition 6. With the parameterization $\epsilon_\theta(\mathbf{u}, t) = -\mathbf{R}_t^T s_\theta(\mathbf{u}, t)$ and the approximator $\tilde{\epsilon}_\theta(\mathbf{u}, t)$ in Eq (19), the solution to Eq (6) satisfies

$$\mathbf{u}(t) \sim \mathcal{N}(\Psi(t, s)\mathbf{u}(s) + [\hat{\Psi}(t, s) - \Psi(t, s)] \mathbf{R}_s \epsilon_\theta(\mathbf{u}(s), s), \mathbf{P}_{st}), \quad (20)$$

where $\hat{\Psi}(t, s)$ is the transition matrix associated with $\hat{\mathbf{F}}_\tau := \mathbf{F}_\tau + \frac{1+\lambda^2}{2} \mathbf{G}_\tau \mathbf{G}_\tau^T \Sigma_\tau^{-1}$ and the covariance matrix \mathbf{P}_{st} solves

$$\frac{d\mathbf{P}_{s\tau}}{d\tau} = \hat{\mathbf{F}}_\tau \mathbf{P}_{s\tau} + \mathbf{P}_{s\tau} \hat{\mathbf{F}}_\tau^T + \lambda^2 \mathbf{G}_\tau \mathbf{G}_\tau^T, \quad \mathbf{P}_{ss} = 0. \quad (21)$$

Our stochastic gDDIM then uses Eq (20) for update. Interestingly, though look quite different between stochastic gDDIM and deterministic gDDIM, there exists a connection when $\lambda = 0$,

Proposition 7. Eq (20) in stochastic gDDIM reduces to Eq (16) in deterministic gDDIM when $\lambda = 0$.

4.3 Training and accelerating CLD

We illustrate the gDDIM that is applicable to any DMs with a case study over CLD. Denote by $\epsilon_\theta(\mathbf{u}, t) = [\epsilon_\theta(\mathbf{u}, t; \mathbf{x}), \epsilon_\theta(\mathbf{u}, t; \mathbf{v})]$ for corresponding model parameterization. The authors of Dockhorn et al. [5] originally propose the parameterization $s_\theta(\mathbf{u}, t) = -\mathbf{L}_t^{-T} \epsilon_\theta(\mathbf{u}, t)$ where $\Sigma_t = \mathbf{L}_t \mathbf{L}_t^T$ is the Cholesky decomposition of the covariance matrix of $p_{0t}(\mathbf{u}(t)|\mathbf{x}(0))$. Built on DSM Eq (3), they propose *hybrid score matching (HSM)* that is claimed to be advantageous [5]. It uses the loss

$$\mathbb{E}_{t \sim \mathcal{U}[0, T]} \mathbb{E}_{\mathbf{x}(0), \mathbf{u}(t) | \mathbf{x}(0)} [\|\epsilon - \epsilon_\theta(\mu_t(\mathbf{x}_0) + \mathbf{L}_t \epsilon, t)\|_{\mathbf{L}_t^{-1} \Lambda_t \mathbf{L}_t^{-T}}^2]. \quad (22)$$

With a similar derivation [5], we obtain the HSM loss with our new score parameterization $s_\theta(\mathbf{u}, t) = -\mathbf{L}_t^{-T} \epsilon_\theta(\mathbf{u}, t)$ as

$$\mathbb{E}_{t \sim \mathcal{U}[0, T]} \mathbb{E}_{\mathbf{x}(0), \mathbf{u}(t) | \mathbf{x}(0)} [\|\epsilon - \epsilon_\theta(\mu_t(\mathbf{x}_0) + \mathbf{R}_t \epsilon, t)\|_{\mathbf{R}_t^{-1} \Lambda_t \mathbf{R}_t^{-T}}^2]. \quad (23)$$

Though Eq (22) and (23) look similar, we cannot directly use pretrained model provided in Dockhorn et al. [5] for gDDIM. Due to the lower triangular structure of \mathbf{L}_t and the special \mathbf{G}_t , the solution to Eq (6) only relies on $\epsilon_\theta(\mathbf{u}, t; \mathbf{v})$ and thus only $\epsilon_\theta(\mathbf{u}, t; \mathbf{v})$ is learned in Dockhorn et al. [5] via a special choice of Λ_t . In contrast, in our new parametrization, both $\epsilon_\theta(\mathbf{u}, t; \mathbf{x})$ and $\epsilon_\theta(\mathbf{u}, t; \mathbf{v})$ are needed to solve Eq (6). To train score model for gDDIM, we set $\mathbf{R}_t^{-1} \Lambda_t \mathbf{R}_t^{-T} = \mathbf{I}$ for simplicity, similar to the choice made in Ho et al. [6]. Our weight choice has reasonable performance and we leave improvement possibilities, such as mixed score [5], better Λ_t weights [32], for future work. Though we requires a different training scheme of score model compared with Dockhorn et al. [5], the modifications on the training pipeline and extra costs are almost ignorable. We include more discussions in Appendix C.

5 Experiments

We validate the effectiveness of gDDIM on CLD. We design experiments to answer the following questions. How to verify Prop 4 and 5 empirically? Can gDDIM improve sampling efficiency compared with existing works? What differences does the choice of λ and \mathbf{K}_t make? We present sampling results on CIFAR10. (Implementation details and more experiments are included in Appendix C)

Choice of \mathbf{K}_t : \mathbf{L}_t vs \mathbf{R}_t . A key of gDDIM is the special choice $\mathbf{K}_t = \mathbf{R}_t$ which is obtained via solving Eq (15). In CLD, \mathbf{L}_t [5] does not obey Eq (15) and $\mathbf{L}_t \neq \mathbf{R}_t$. As it is shown in Fig 1, on real datasets with trained score model, we randomly pick pixel locations and check the pixel value and ϵ_θ output along the solutions to the probability flow ODE produced by high resolution ODE solver. With the choice $\mathbf{K}_t = \mathbf{L}_t$, $\epsilon_\theta^{(L)}(\mathbf{u}, t; \mathbf{v})$ suffers from oscillation like \mathbf{x} value along time. However, $\epsilon_\theta^{(R)}(\mathbf{u}, t)$ is much more flat. We further compare samples generated by \mathbf{L}_t and \mathbf{R}_t parameterization in Tab 1.

Table 1: \mathbf{L}_t vs \mathbf{R}_t

	FID at different NFE			
\mathbf{K}_t	20	30	40	50
\mathbf{L}_t	364	157	4.02	3.24
\mathbf{R}_t	3.90	2.66	2.39	2.28

Table 2: λ and integrators choice with NFE=50

	FID at different λ					
Method	0.0	0.1	0.3	0.5	0.7	1.0
gDDIM	5.38	5.6	13.12	32	42	48
EM	346	169	141	94	41	57

Choice of λ : ODE vs SDE. We further conduct comparison study with different λ values. Note that polynomial extrapolation in Eq (17) is not used here even when $\lambda = 0$. As it is shown in Tab 2, increasing λ deteriorates the sample quality, demonstrating our claim that deterministic DDIM has better performance than its stochastic counterpart when a small NFE is used. We also find stochastic gDDIM significantly outperforms EM integrator.

6 Conclusion and Broader Impact

Contribution: The more structural knowledge we take advantage, the more efficient we are. In this work, we provide a clean interpretation of DDIMs based on the manifold hypothesis and the sparsity property on realistic dataset. This new perspective unboxes the numerical discretization used in DDIM and explains the advantage of ODE-based sampler over SDE-based when NFE is small. Based on this interpretation, we extend DDIMs to general diffusion models. The new algorithm, gDDIM, only conducts a tiny but elegant modification on the parameterization of score model and improves in sampling efficiency drastically. We conduct extensive experiments to validate the effectiveness of our new sampling algorithm and achieve encouraging results when apply gDDIM in CLD models.

Limitation: There are several promising future directions. First, though gDDIM is designed for general DMs, we only verify it on CLD model in addition to DDPM. gDDIM-based CLD shows better image sampling quality under 50 NFE but still cannot produce satisfying results when NFE is extreme small, e.g. 10 or 5 steps. It is beneficial to explore more efficient diffusion process for

Table 3: Unconditional CIFAR10 generative performance

Class	Model	NFE (\downarrow)	FID (\downarrow)
CLD	our CLD-SGM (gDDIM)	50	2.28
	our CLD-SGM (SDE, EM)	2000	2.43
	our CLD-SGM (Prob.Flow, RK45)	157	3.16
	CLD-SGM (Prob.Flow, RK45) by Dockhorn et al. [5]	147	2.71
	CLD-SGM (SDE, EM) by Dockhorn et al. [5]	2000	2.23
Score	NCSN by Song & Ermon [29]	1000	25.3
	DDPM by Ho et al. [6]	1000	3.17
	D3PMs by Austin et al. [2]	1000	7.34
	DDPM++, VP by Song et al. [31]	2000	2.41
	DDPM++, sub-VP by Song et al. [31]	2000	2.41
	NCSN++ by Song et al. [31]	2000	2.20
	Likelihood SDE by Song et al. [32]	-	2.87
	Improved DDPM by Nichol & Dhariwal [17]	4000	2.90
	UDM by Kim et al. [11]	2000	2.33
Score+Others	LSGM by Vahdat et al. [35]	138	2.10
	LSGM-100M by Vahdat et al. [35]	131	4.60
	Diffusion GAN by Xiao et al. [40]	4	3.75

Table 4: Efficiency comparison among training-free samplers, FID / NFE on CIFAR10

DDIM [28]	FastDPM [13]	DEIS [42]	PNDM [14]	ADDIM [3]	gDDIM
13.36 / 10	9.90 / 10	4.17 / 10	7.05/19	14.0/10	13.41 / 10
6.87 / 20	5.05 / 20	3.31 / 20	4.61/29	5.81/20	3.90 / 20
4.47 / 50	3.32 / 50	2.99 / 50	3.68/59	4.04/50	2.87 / 27
4.16 / 100	2.86 /100	-	3.53/109	3.55/100	2.28 / 50

different datasets, in which we believe gDDIM will play a important role in designing sampling algorithm. Second, more investigation are needed to design efficient sampling algorithm by exploiting more structural knowledge in DMs. The structural knowledge can originate from different sources such as different modality of datasets, and mathematical structure presented in specific diffusion processes. An interesting question for further improving CLD stochastic sampling is how to take advantage of the fact that gDDIM has a conservative Hamiltonian component, in addition to noise, friction, and forcing from the score.

References

- [1] Anderson, B. D. Reverse-time diffusion equation models. *Stochastic Process. Appl.*, 12 (3):313–326, May 1982. ISSN 0304-4149. doi: 10.1016/0304-4149(82)90051-5. URL [https://doi.org/10.1016/0304-4149\(82\)90051-5](https://doi.org/10.1016/0304-4149(82)90051-5).
- [2] Austin, J., Johnson, D. D., Ho, J., Tarlow, D., and van den Berg, R. Structured denoising diffusion models in discrete state-spaces. *Advances in Neural Information Processing Systems*, 34:17981–17993, 2021.
- [3] Bao, F., Li, C., Zhu, J., and Zhang, B. Analytic-DPM: An Analytic Estimate of the Optimal Reverse Variance in Diffusion Probabilistic Models. 2022. URL <http://arxiv.org/abs/2201.06503>.
- [4] Dhariwal, P. and Nichol, A. Diffusion Models Beat GANs on Image Synthesis. 2021. URL <http://arxiv.org/abs/2105.05233>.
- [5] Dockhorn, T., Vahdat, A., and Kreis, K. Score-Based Generative Modeling with Critically-Damped Langevin Diffusion. pp. 1–13, 2021. URL <http://arxiv.org/abs/2112.07068>.
- [6] Ho, J., Jain, A., and Abbeel, P. Denoising diffusion probabilistic models. In *Advances in Neural Information Processing Systems*, volume 2020-Decem, 2020. ISBN 2006.11239v2. URL <https://github.com/hojonathanho/diffusion>.
- [7] Hochbruck, M. and Ostermann, A. Exponential integrators. *Acta Numerica*, 19:209–286, 2010.
- [8] Jolicœur-Martineau, A., Li, K., Piché-Taillefer, R., Kachman, T., and Mitliagkas, I. Gotta go fast when generating data with score-based models. *arXiv preprint arXiv:2105.14080*, 2021.
- [9] Jolicœur-Martineau, A., Li, K., Pich{\'e}-Taillefer, R., Kachman, T., and Mitliagkas, I. Gotta Go Fast When Generating Data with Score-Based Models. May 2021. doi: 10.48550/arxiv.2105.14080. URL <http://arxiv.org/abs/2105.14080>.
- [10] Kavar, B., Vaksman, G., and Elad, M. Snips: Solving noisy inverse problems stochastically. *Advances in Neural Information Processing Systems*, 34, 2021.
- [11] Kim, D., Shin, S., Song, K., Kang, W., and Moon, I.-C. Score matching model for unbounded data score. *arXiv preprint arXiv:2106.05527*, 2021.
- [12] Kong, Z. and Ping, W. On Fast Sampling of Diffusion Probabilistic Models. 2021. URL <http://arxiv.org/abs/2106.00132>.
- [13] Kong, Z. and Ping, W. On fast sampling of diffusion probabilistic models. *arXiv preprint arXiv:2106.00132*, 2021.
- [14] Liu, L., Ren, Y., Lin, Z., and Zhao, Z. Pseudo Numerical Methods for Diffusion Models on Manifolds. (2021):1–23, 2022. URL <http://arxiv.org/abs/2202.09778>.
- [15] Luhman, E. and Luhman, T. Knowledge distillation in iterative generative models for improved sampling speed. *arXiv preprint arXiv:2101.02388*, 2021.
- [16] Lyu, S. Interpretation and generalization of score matching. *arXiv preprint arXiv:1205.2629*, 2012.
- [17] Nichol, A. and Dhariwal, P. Improved denoising diffusion probabilistic models. *ArXiv*, abs/2102.09672, 2021.
- [18] Nichol, A., Dhariwal, P., Ramesh, A., Shyam, P., Mishkin, P., McGrew, B., Sutskever, I., and Chen, M. GLIDE: Towards Photorealistic Image Generation and Editing with Text-Guided Diffusion Models. 2021. URL <http://arxiv.org/abs/2112.10741>.
- [19] Oksendal, B. *Stochastic differential equations: an introduction with applications*. Springer Science & Business Media, 2013.
- [20] Press, W. H., Teukolsky, S. A., Vetterling, W. T., and Flannery, B. P. *Numerical recipes 3rd edition: The art of scientific computing*. Cambridge university press, 2007.
- [21] Ramesh, A., Dhariwal, P., Nichol, A., Chu, C., and {Chen OpenAI}, M. Hierarchical Text-Conditional Image Generation with CLIP Latents.
- [22] Rombach, R., Blattmann, A., Lorenz, D., Esser, P., and Ommer, B. High-Resolution Image Synthesis with Latent Diffusion Models. 2021. URL <http://arxiv.org/abs/2112.10752>.

- [23] Roweis, S. T. and Saul, L. K. Nonlinear dimensionality reduction by locally linear embedding. *Science*, 290 5500:2323–6, 2000.
- [24] Salimans, T. and Ho, J. Progressive Distillation for Fast Sampling of Diffusion Models. 2022. URL <http://arxiv.org/abs/2202.00512>.
- [25] Särkkä, S. and Solin, A. *Applied stochastic differential equations*, volume 10. Cambridge University Press, 2019.
- [26] Sauer, T. Numerical analysis, 2005.
- [27] Sohl-Dickstein, J., Weiss, E., Maheswaranathan, N., and Ganguli, S. Deep unsupervised learning using nonequilibrium thermodynamics. In *International Conference on Machine Learning*, pp. 2256–2265. PMLR, 2015.
- [28] Song, J., Meng, C., and Ermon, S. Denoising Diffusion Implicit Models. 2020. URL <http://arxiv.org/abs/2010.02502>.
- [29] Song, Y. and Ermon, S. Generative modeling by estimating gradients of the data distribution. *Advances in Neural Information Processing Systems*, 32, 2019.
- [30] Song, Y., Sohl-Dickstein, J., Kingma, D. P., Kumar, A., Ermon, S., and Poole, B. Score-Based Generative Modeling through Stochastic Differential Equations. 2020. URL <http://arxiv.org/abs/2011.13456>.
- [31] Song, Y., Sohl-Dickstein, J., Kingma, D. P., Kumar, A., Ermon, S., and Poole, B. Score-Based Generative Modeling through Stochastic Differential Equations. *ArXiv preprint*, abs/2011.13456, 2020. URL <https://arxiv.org/abs/2011.13456>.
- [32] Song, Y., Durkan, C., Murray, I., and Ermon, S. Maximum likelihood training of score-based diffusion models. *Advances in Neural Information Processing Systems*, 34, 2021.
- [33] Tachibana, H., Go, M., Inahara, M., Katayama, Y., and Watanabe, Y. Itô-taylor sampling scheme for denoising diffusion probabilistic models using ideal derivatives. *arXiv preprint arXiv:2112.13339*, 2021.
- [34] Tenenbaum, J. B., Silva, V. D., and Langford, J. C. A global geometric framework for nonlinear dimensionality reduction. *Science*, 290 5500:2319–23, 2000.
- [35] Vahdat, A., Kreis, K., and Kautz, J. Score-based generative modeling in latent space. In *Neural Information Processing Systems (NeurIPS)*, 2021.
- [36] Vincent, P. A connection between score matching and denoising autoencoders. *Neural Comput.*, 23(7):1661–1674, July 2011. ISSN 0899-7667, 1530-888X. doi: 10.1162/neco_a_00142. URL https://doi.org/10.1162/neco_a_00142.
- [37] Watson, D., Ho, J., Norouzi, M., and Chan, W. Learning to efficiently sample from diffusion probabilistic models. *arXiv preprint arXiv:2106.03802*, 2021.
- [38] Watson, D., Chan, W., Ho, J., and Norouzi, M. Learning Fast Samplers for Diffusion Models by Differentiating Through Sample Quality. 2022. URL <http://arxiv.org/abs/2202.05830>.
- [39] Whalen, P., Brio, M., and Moloney, J. Exponential time-differencing with embedded Runge–Kutta adaptive step control. *J. Comput. Phys.*, 280:579–601, January 2015. ISSN 0021-9991. doi: 10.1016/j.jcp.2014.09.038. URL <https://doi.org/10.1016/j.jcp.2014.09.038>.
- [40] Xiao, Z., Kreis, K., and Vahdat, A. Tackling the generative learning trilemma with denoising diffusion gans. *arXiv preprint arXiv:2112.07804*, 2021.
- [41] Zhang, Q. and Chen, Y. Diffusion normalizing flow. *Advances in Neural Information Processing Systems*, 34, 2021.
- [42] Zhang, Q. and Chen, Y. Fast sampling of diffusion models with exponential integrator. *arXiv preprint arXiv:2204.13902*, 2022.

A More related works

Learning generative models with DMs via score matching has received tremendous attention recently [27, 16, 29, 30, 6, 17]. However, the sampling efficiency of DMs is still not satisfying. Jolicœur-Martineau et al. [8] introduced adaptive solver for SDEs associated with DMs for the task of image generation. Song et al. [28] modified the forward noising process into a non-Markov process without changing the training objective function. The authors then proposed a family of samplers, including deterministic DDIM and stochastic DDIM, based on the modifications. Both of the samplers demonstrate significant improvements over previous samplers. There are variants of the DDIM that aim to further improve the sampling quality and efficiency. Bao et al. [3] improved the DDIM by optimizing the reverse variance in DMs. Watson et al. [38] generalized the DDIM in DDPM with learned update coefficients, which is trained by minimizing an external perceptual loss. Nichol & Dhariwal [17] tuned the variance of schedule of DDPM. Liu et al. [14] found that the DDIM is a pseudo numerical method and proposed a pseudo linear multi-step method for it. Zhang & Chen [42] discovered that DDIMs are numerical integrators for marginal-equivalent SDEs, and the deterministic DDIM is actually an exponential integrator for the probability flow ODE. They further utilized exponential multistep methods to boost sampling performance for VPSDE.

Another promising approach to accelerate diffusion model is distillation for the probability flow ODE. Luhman & Luhman [15] proposed to learn the map from noise to data in a teacher-student fashion, where supervised signals are provided by simulating the deterministic DDIM. The final student network distilled is able to generate samples with reasonable quality within one step. Salimans & Ho [24] proposed a new progressive distillation approach to improve the training efficiency and stability. This distillation approach relies on solving the probability flow ODE and needs extra training procedure. Since we generalize and improve the DDIM in this work, it will be beneficial to combine this distillation method with our algorithm for better performance in the future.

Recently, numerical structures of DMs have received more and more attentions; they play important roles in efficient sampling methods. Dockhorn et al. [5] designed Symmetric Splitting CLD Sampler (SSCS) that takes advantage of Hamiltonian structure of the CLD and demonstrated advantages over the naive Euler-Maruyama method. Zhang & Chen [42] utilized the semilinear structure presented in DMs and showed that the exponential integrator gave much better sampling quality than Euler method. Further tailoring these integrators to account for the stiff property of ODEs [7, 39] is a promising direction in fast sampling for DMs.

B Proofs

Since the proposed gDDIM is a generalization of DDIM, the results regarding gDDIM in Section 4 are generalizations of those in Section 3. In particular, Prop 4 generalizes Prop 1, Eq (16) generalizes Prop 2, and Prop 5 generalizes Prop 3. Thus, for the sake of simplicity, we mainly present proofs for gDDIM in Section 4.

B.1 Deterministic gDDIM

B.1.1 Proof of Eq (15)

Since we assume data distribution $p_0(\mathbf{u}) = \mathcal{N}(\mathbf{u}_0, \Sigma_0)$, the score has closed form

$$\nabla \log p_t(\mathbf{u}) = -\Sigma_t^{-1}(\mathbf{u} - \Psi(t, 0)\mathbf{u}_0). \quad (24)$$

To make sure our construction Eq (14) is a solution to the probability flow ODE, we examine the condition for \mathbf{R}_t . The LHS of the probability flow ODE is

$$\begin{aligned} d\mathbf{u} &= d[\Psi(t, 0)\mathbf{u}_0 + \mathbf{R}_t\epsilon] \\ &= \dot{\Psi}(t, 0)\mathbf{u}_0 dt + \dot{\mathbf{R}}_t\epsilon dt \\ &= [\mathbf{F}_t\Psi(t, 0)\mathbf{u}_0 + \dot{\mathbf{R}}_t\epsilon]dt. \end{aligned} \quad (25)$$

The RHS of the probability flow ODE is

$$\begin{aligned} [\mathbf{F}_t \mathbf{u} - \frac{1}{2} \mathbf{G}_t \mathbf{G}_t^T \nabla \log p_t(\mathbf{u})] dt &= [\mathbf{F}_t \Psi(t, 0) \mathbf{u}_0 + \mathbf{F}_t \mathbf{R}_t \epsilon + \frac{1}{2} \mathbf{G}_t \mathbf{G}_t^T \mathbf{R}_t^{-T} \epsilon] dt \\ &= [\mathbf{F}_t \Psi(t, 0) \mathbf{u}_0 + \mathbf{F}_t \mathbf{R}_t \epsilon + \frac{1}{2} \mathbf{G}_t \mathbf{G}_t^T \mathbf{R}_t^{-T} \mathbf{R}_t^{-1} \mathbf{R}_t \epsilon] dt, \end{aligned} \quad (26)$$

where the first equality is due to $\nabla \log p_t(\mathbf{u}) = -\mathbf{R}_t^{-T} \epsilon$.

Since Eq (25) and (26) holds for each ϵ , we establish

$$\dot{\mathbf{R}}_t = (\mathbf{F}_t + \frac{1}{2} \mathbf{G}_t \mathbf{G}_t^T \mathbf{R}_t^{-T} \mathbf{R}_t^{-1}) \mathbf{R}_t \quad (27)$$

$$= (\mathbf{F}_t + \frac{1}{2} \mathbf{G}_t \mathbf{G}_t^T \Sigma_t^{-1}) \mathbf{R}_t. \quad (28)$$

B.1.2 Proof of Prop 4

Similar to the proof of Eq (15), over a solution $\{\mathbf{u}(t), t\}$ to the probability flow ODE, $\mathbf{R}^{-1}(\mathbf{u}(t) - \Psi(t, 0) \mathbf{u}_0)$ is constant. Furthermore, by Eq (24),

$$\begin{aligned} \nabla \log p_t(\mathbf{u}(t)) &= -\Sigma_t^{-1}(\mathbf{u}(t) - \Psi(t, 0) \mathbf{u}_0) \\ &= -\mathbf{R}_t^{-T} \mathbf{R}_t^{-1}(\mathbf{u}(t) - \Psi(t, 0) \mathbf{u}_0) \end{aligned} \quad (29)$$

Eq (29) implies that $-\mathbf{R}_t^T \nabla \log p_t(\mathbf{u}(t))$ is a constant and invariant with respect to t .

B.1.3 Proof of Eq (11) and (16)

We derive Eq (16) first.

The update step is based on the approximation $\tilde{\epsilon}_\theta(\mathbf{u}, \tau) = \epsilon_\theta(\mathbf{u}(t), t)$ for $\tau \in [t - \Delta t, t]$. The resulted ODE with $\tilde{\epsilon}_\theta$ reads

$$\dot{\mathbf{u}} = \mathbf{F}_\tau \mathbf{u} + \frac{1}{2} \mathbf{G}_\tau \mathbf{G}_\tau^T \mathbf{R}_\tau^{-1} \epsilon_\theta(\mathbf{u}(t), t), \quad (30)$$

which is a linear ODE. The closed-form solution reads

$$\mathbf{u}(t_{i-1}) = \Psi(t_{i-1}, t_i) \mathbf{u}(t) + \left[\int_{t_i}^{t_{i-1}} \frac{1}{2} \Psi(t_{i-1}, \tau) \mathbf{G}_\tau \mathbf{G}_\tau^T \mathbf{R}_\tau^{-T} \right] \epsilon_\theta(\mathbf{u}(t), t), \quad (31)$$

where $\Psi(t, s)$ is the transition matrix associated \mathbf{F}_t , that is, Ψ satisfies

$$\frac{d\Psi(t, s)}{dt} = \mathbf{F}_t \Psi(t, s) \quad \Psi(s, s) = \mathbf{I}_D. \quad (32)$$

When the DM is specified to be DDPM, we derive Eq (11) based on Eq (16) by expanding the coefficients in Eq (16) explicitly as

$$\begin{aligned} \Psi(t, s) &= \sqrt{\frac{\alpha_t}{\alpha_s}}, \\ \Psi(t - \Delta t, t) &= \sqrt{\frac{\alpha_{t-\Delta t}}{\alpha_t}}, \\ \int_t^{t-\Delta t} \frac{1}{2} \Psi(t - \Delta t, \tau) \mathbf{G}_\tau \mathbf{G}_\tau^T \mathbf{R}_\tau^{-1} d\tau &= \int_t^{t-\Delta t} -\frac{1}{2} \sqrt{\frac{\alpha_{t-\Delta t}}{\alpha_\tau}} \frac{d \log \alpha_\tau}{d\tau} \frac{1}{\sqrt{1 - \alpha_\tau}} d\tau \\ &= \sqrt{\alpha_{t-\Delta t}} \sqrt{\frac{1 - \alpha_\tau}{\alpha_\tau}} \Big|_{\alpha_t}^{\alpha_{t-\Delta t}} \\ &= \sqrt{1 - \alpha_{t-\Delta t}} - \sqrt{1 - \alpha_t} \sqrt{\frac{\alpha_{t-\Delta t}}{\alpha_t}}. \end{aligned}$$

B.1.4 Proof of Multistep Predictor-Corrector

Our Multistep Predictor-Corrector method slightly extends the traditional linear multistep Predictor-Corrector method to incorporate the semilinear structure in the probability flow ODE with an exponential integrator [20, 7].

Predictor:

For Eq (7), the key insight of the multistep predictor is to use existing function evaluations $\epsilon_\theta(\mathbf{u}(t_i), t_i), \epsilon_\theta(\mathbf{u}(t_{i+1}), t_{i+1}), \dots, \epsilon_\theta(\mathbf{u}(t_{i+q-1}), t_{i+q-1})$ and their timestamps $t_i, t_{i+1}, \dots, t_{i+q-1}$ to fit a $q-1$ order polynomial ${}^p\epsilon_\theta(t)$ to approximate $\epsilon_\theta(\mathbf{u}(\tau), \tau)$. With this approximator $\tilde{\epsilon}_\theta(\mathbf{u}, \tau) = {}^p\epsilon_\theta(\tau)$ for $\tau \in [t_{i-1}, t_i]$, the multistep predictor step is obtained by solving

$$\begin{aligned} \frac{d\mathbf{u}}{dt} &= \mathbf{F}_t \mathbf{u} + \frac{1}{2} \mathbf{G}_\tau \mathbf{G}_\tau^T \mathbf{R}_\tau^{-T} \tilde{\epsilon}_\theta(\mathbf{u}, \tau) \\ &= \mathbf{F}_t \mathbf{u} + \frac{1}{2} \mathbf{G}_\tau \mathbf{G}_\tau^T \mathbf{R}_\tau^{-T} {}^p\epsilon_\theta(\tau), \end{aligned} \quad (33)$$

which is a linear ODE. The solution to Eq (33) satisfies

$$\mathbf{u}(t_{i-1}) = \Psi(t_{i-1}, t_i) \mathbf{u}(t_i) + \int_{t_i}^{t_{i-1}} \frac{1}{2} \mathbf{G}_\tau \mathbf{G}_\tau^T \mathbf{R}_\tau^{-T} {}^p\epsilon_\theta(\tau) d\tau. \quad (34)$$

Based on Lagrange formula, we can write ${}^p\epsilon_\theta(\tau)$ as

$${}^p\epsilon_\theta(\tau) = \sum_{j=0}^{q-1} \left[\prod_{k \neq j} \frac{\tau - t_{i+k}}{t_{i+j} - t_{i+k}} \right] \epsilon_\theta(\mathbf{u}_{t_{i+j}}, t_{i+j}). \quad (35)$$

Plugging Eq (35) into Eq (34), we obtain

$$\mathbf{u}(t_{i-1}) = \Psi(t_{i-1}, t_i) \mathbf{u}(t_i) + \sum_{j=0}^{q-1} [{}^p\mathbf{C}_{ij}^{(q)} \epsilon_\theta(\mathbf{u}(t_{i+j}), t_{i+j})], \quad (36)$$

$${}^p\mathbf{C}_{ij}^{(q)} = \int_{t_i}^{t_{i-1}} \frac{1}{2} \Psi(t_{i-1}, \tau) \mathbf{G}_\tau \mathbf{G}_\tau^T \mathbf{R}_\tau^{-T} \prod_{k \neq j, k=0}^{q-1} \left[\frac{\tau - t_{i+k}}{t_{i+j} - t_{i+k}} \right] d\tau, \quad (37)$$

which are Eq (17a) and (17b). Here we use ${}^p\mathbf{C}_{ij}^{(q)}$ to emphasis these are constants used in the q -step predictor. The 1-step predictor reduces to Eq (16).

Corrector:

Compared with the explicit scheme for the multistep predictor, the multistep corrector behaves like an implicit method [20]. Instead of constructing ${}^p\epsilon_\theta(\tau)$ to extrapolate model output for $\tau \in [t_{i-1}, t_i]$ as in the predictor, the q step corrector aims to find ${}^c\epsilon_\theta(\tau)$ to interpolate $\epsilon_\theta(\mathbf{u}(t_{i-1}), t_{i-1}), \epsilon_\theta(\mathbf{u}(t_i), t_i), \epsilon_\theta(\mathbf{u}(t_{i+1}), t_{i+1}), \dots, \epsilon_\theta(\mathbf{u}(t_{i+q-2}), t_{i+q-2})$ and their timestamps $t_{i-1}, t_i, t_{i+1}, \dots, t_{i+q-2}$. Thus, $\mathbf{u}(t_{i-1})$ is obtained by solving

$$\mathbf{u}(t_{i-1}) = \Psi(t_{i-1}, t_i) \mathbf{u}(t_i) + \int_{t_i}^{t_{i-1}} \frac{1}{2} \mathbf{G}_\tau \mathbf{G}_\tau^T \mathbf{R}_\tau^{-T} {}^c\epsilon_\theta(\tau) d\tau. \quad (38)$$

Since ${}^c\epsilon_\theta(\tau)$ is defined implicitly, it is not easy to find ${}^c\epsilon_\theta(\tau), \mathbf{u}(t_{i-1})$. Instead, practitioners bypass the difficulties by interpolating $\epsilon_\theta(\bar{\mathbf{u}}(t_{i-1}), t_{i-1}), \epsilon_\theta(\bar{\mathbf{u}}(t_i), t_i), \epsilon_\theta(\bar{\mathbf{u}}(t_{i+1}), t_{i+1}), \dots, \epsilon_\theta(\bar{\mathbf{u}}(t_{i+q-2}), t_{i+q-2})$ where $\bar{\mathbf{u}}(t_{i-1})$ is obtained by the predictor in Eq (34) and $\bar{\mathbf{u}}(t_i) = \mathbf{u}(t_i), \bar{\mathbf{u}}(t_{i+1}) = \mathbf{u}(t_{i+1}), \dots, \bar{\mathbf{u}}(t_{i+q-2}) = \mathbf{u}(t_{i+q-2})$. Hence, we derive the update step for corrector based on

$$\mathbf{u}(t_{i-1}) = \Psi(t_{i-1}, t_i) \mathbf{u}(t_i) + \int_{t_i}^{t_{i-1}} \frac{1}{2} \mathbf{G}_\tau \mathbf{G}_\tau^T \mathbf{R}_\tau^{-T} {}^c\epsilon_\theta(\tau) d\tau, \quad (39)$$

where ${}^c\epsilon_\theta(\tau)$ is defined as

$${}^c\epsilon_\theta(\tau) = \sum_{j=-1}^{q-2} \left[\prod_{k \neq j} \frac{\tau - t_{i+k}}{t_{i+j} - t_{i+k}} \right] \epsilon_\theta(\bar{\mathbf{u}}_{t_{i+j}}, t_{i+j}). \quad (40)$$

Plugging Eq (40) into Eq (39), we reach the update step for the corrector

$$\mathbf{u}(t_{i-1}) = \Psi(t_{i-1}, t_i) \mathbf{u}(t_i) + \sum_{j=-1}^{q-2} [{}^c\mathbf{C}_{ij}^{(q)} \epsilon_{\theta}(\bar{\mathbf{u}}(t_{i+j}), t_{i+j})], \quad (41)$$

$${}^c\mathbf{C}_{ij}^{(q)} = \int_{t_i}^{t_{i-1}} \frac{1}{2} \Psi(t_{i-1}, \tau) \mathbf{G}_{\tau} \mathbf{G}_{\tau}^T \mathbf{R}_{\tau}^{-T} \prod_{k \neq j, k=-1}^{q-2} \left[\frac{\tau - t_{i+k}}{t_{i+j} - t_{i+k}} \right] d\tau. \quad (42)$$

We use ${}^c\mathbf{C}_{ij}^{(q)}$ to emphasis constants used in the q -step corrector.

Exponential multistep Predictor-Corrector:

Here we present the Exponential multistep Predictor-Corrector algorithm. Specifically, we employ one q -step corrector update step after an update step of the q -step predictor. The interested reader can easily extend the idea to employ multiple update steps of corrector or different number of steps for the predictor and the corrector. We note coefficients ${}^p\mathbf{C}$, ${}^c\mathbf{C}$ can be calculated using high resolution ODE solver once and used everywhere.

Algorithm 1 Exponential multistep Predictor-Corrector

Input: Timestamps $\{t_i\}_{i=0}^N$, step order q , coefficients for predictor update ${}^p\mathbf{C}$, coefficients for corrector update ${}^c\mathbf{C}$
Instantiate: $\mathbf{u}(t_N) \sim p_T(\mathbf{u})$
for i in $N, N-1, \dots, 1$ **do**
 # predictor update step
 $q_{\text{cur}} = \min(q, N-i+1)$ # handle warming start, use lower order multistep method
 $\mathbf{u}_{t_{i-1}} \leftarrow \text{Simulate Eq (36) with } q_{\text{cur}}\text{-step predictor}$
 # corrector update step
 $q_{\text{cur}} = \min(q, N-i+2)$ # handle warming start, use lower order multistep method
 $\bar{\mathbf{u}}(t_{i-1}), \bar{\mathbf{u}}(t_i), \dots, \bar{\mathbf{u}}(t_{i+q_{\text{cur}}-1}) \leftarrow \mathbf{u}(t_{i-1}), \mathbf{u}(t_i), \dots, \mathbf{u}(t_{i+q_{\text{cur}}-1})$
 $\mathbf{u}_{t_{i-1}} \leftarrow \text{Simulate Eq (41) with } q_{\text{cur}}\text{-step corrector}$
end for

B.2 Stochastic gDDIM

B.2.1 Proof of Prop 5

Assuming that the data distribution $p_0(\mathbf{u})$ is $\mathcal{N}(\mathbf{u}_0, \Sigma_0)$ with a given Σ_0 , we can derive the mean and covariance of $p_t(\mathbf{u})$ as

$$\mu_t = \Psi(t, 0) \quad (43)$$

$$\frac{d\Sigma_t}{dt} = \mathbf{F}_t \Sigma_t + \Sigma_t \mathbf{F}_t^T + \mathbf{G}_t \mathbf{G}_t^T. \quad (44)$$

Therefore, the ground truth score reads

$$\nabla \log p_t(\mathbf{u}) = -\Sigma_t^{-1}(\mathbf{u} - \Psi(t, 0)\mathbf{u}_0). \quad (45)$$

We assume Σ_0 is given but \mathbf{u}_0 is unknown. Fortunately, \mathbf{u}_0 can be inferred via one score evaluation as follows. Given evaluation $\nabla \log p_s(\mathbf{u}(s))$, we can recover \mathbf{u}_0 as

$$\mathbf{u}_0 = \Psi(0, s)[\Sigma_s \nabla \log p_s(\mathbf{u}(s)) + \mathbf{u}(s)]. \quad (46)$$

Plugging Eq (46) and $\Psi(t, s) = \Psi(t, 0)\Psi(0, s)$ into Eq (45), we recover Eq (18).

B.2.2 Proof of Prop 6

With the approximator $\tilde{\epsilon}_\theta(\mathbf{u}, t)$ defined in Eq (19) for $\tau \in [s, t]$, Eq (6) can be reformulated as

$$\begin{aligned} d\mathbf{u} &= \mathbf{F}_\tau \mathbf{u} d\tau + \frac{1+\lambda^2}{2} \mathbf{G}_\tau \mathbf{G}_\tau^T \mathbf{R}_\tau^{-T} \tilde{\epsilon}_\theta(\mathbf{u}, \tau) dt + \lambda \mathbf{G}_\tau d\mathbf{w} \\ &= (\mathbf{F}_\tau + \frac{1+\lambda^2}{2} \mathbf{G}_\tau \mathbf{G}_\tau^T \mathbf{R}_\tau^{-T} \mathbf{R}_\tau^{-1}) \mathbf{u} dt \\ &\quad + \frac{1+\lambda^2}{2} \mathbf{G}_\tau \mathbf{G}_\tau^T \mathbf{R}_\tau^{-T} \mathbf{R}_\tau^{-1} \Psi(\tau, s) (\mathbf{R}_s \epsilon_\theta(\mathbf{u}(s), s) - \mathbf{u}(s)) dt + \lambda \mathbf{G}_\tau d\mathbf{w}. \end{aligned} \quad (47)$$

Define $\hat{\mathbf{F}}_\tau := \mathbf{F}_\tau + \frac{1+\lambda^2}{2} \mathbf{G}_\tau \mathbf{G}_\tau^T \mathbf{R}_\tau^{-T} \mathbf{R}_\tau^{-1} = \mathbf{F}_\tau + \frac{1+\lambda^2}{2} \mathbf{G}_\tau \mathbf{G}_\tau^T \Sigma_\tau^{-1}$, and denote by $\hat{\Psi}(t, s)$ the transition matrix associated with it. Clearly, Eq (47) is a linear differential equation on \mathbf{u} , and the conditional probability $\hat{p}_{st}(\mathbf{u}(t)|\mathbf{u}(s))$ associated with it is a Gaussian distribution.

Applying Särkkä & Solin [25, Eq (6.6,6.7)], we obtain the exact expressions

$$\begin{aligned} \text{Mean} &= \hat{\Psi}(t, s) \mathbf{u}(s) - [\int_s^t \hat{\Psi}(t, \tau) \frac{1+\lambda^2}{2} \mathbf{G}_\tau \mathbf{G}_\tau^T \Sigma_\tau^{-1} \Psi(\tau, s)] d\tau \mathbf{u}(s) \\ &\quad + [\int_s^t \hat{\Psi}(t, \tau) \frac{1+\lambda^2}{2} \mathbf{G}_\tau \mathbf{G}_\tau^T \Sigma_\tau^{-1} \Psi(\tau, s)] d\tau \mathbf{R}_s \epsilon_\theta(\mathbf{u}(s), s) \end{aligned} \quad (48)$$

for the mean of $\hat{p}_{st}(\mathbf{u}(t)|\mathbf{u}(s))$. Its covariance $\mathbf{P}_{s\tau}$ satisfies

$$\frac{d\mathbf{P}_{s\tau}}{d\tau} = \hat{\mathbf{F}}_\tau \mathbf{P}_{s\tau} + \mathbf{P}_{s\tau} \hat{\mathbf{F}}_\tau^T + \lambda^2 \mathbf{G}_\tau \mathbf{G}_\tau^T, \quad \mathbf{P}_{ss} = 0. \quad (49)$$

Eq (48) has a closed form expression with the help of the following lemma.

Lemma 1.

$$\int_s^t \hat{\Psi}(t, \tau) \frac{1+\lambda^2}{2} \mathbf{G}_\tau \mathbf{G}_\tau^T \Sigma_\tau^{-1} \Psi(\tau, s) = \hat{\Psi}(t, s) - \Psi(t, s)$$

Proof. For a fixed s , we define $\mathbf{N}(t) = \int_s^t \hat{\Psi}(t, \tau) \frac{1+\lambda^2}{2} \mathbf{G}_\tau \mathbf{G}_\tau^T \Sigma_\tau^{-1} \Psi(\tau, s)$ and $\mathbf{M}(t) = \hat{\Psi}(t, s) - \Psi(t, s)$. It follows that

$$\begin{aligned} \frac{d\mathbf{N}(\tau)}{d\tau} &= \hat{\mathbf{F}}_\tau \mathbf{N}(\tau) + \frac{1+\lambda^2}{2} \mathbf{G}_\tau \mathbf{G}_\tau^T \Sigma_\tau^{-1} \Psi(\tau, s) \\ &= \mathbf{F}_\tau \mathbf{N}(\tau) + \frac{1+\lambda^2}{2} \mathbf{G}_\tau \mathbf{G}_\tau^T \Sigma_\tau^{-1} [\mathbf{N}(\tau) + \Psi(\tau, s)] \end{aligned} \quad (50)$$

$$\begin{aligned} \frac{d\mathbf{M}(\tau)}{d\tau} &= \hat{\mathbf{F}}_\tau \hat{\Psi}(\tau, s) - \mathbf{F}_\tau \Psi(\tau, s) \\ &= \mathbf{F}_\tau \mathbf{M}(\tau) + \frac{1+\lambda^2}{2} \mathbf{G}_\tau \mathbf{G}_\tau^T \Sigma_\tau^{-1} \hat{\Psi}(\tau, s). \end{aligned} \quad (51)$$

Define $\mathbf{E}(t) = \mathbf{N}(t) - \mathbf{M}(t)$, then

$$\frac{d\mathbf{E}(t)}{dt} = (\mathbf{F}_t + \frac{1+\lambda^2}{2} \mathbf{G}_t \mathbf{G}_t^T \Sigma_t^{-1}) \mathbf{E}(t). \quad (52)$$

On the other hand, $\mathbf{N}(s) = \mathbf{M}(s) = 0$ which implies $\mathbf{E}(s) = 0$. We thus conclude $\mathbf{E}(t) = 0$ and $\mathbf{N}(t) = \mathbf{M}(t)$. \square

Using Lemma 1, we simplify Eq (48) to

$$\Psi(t, s) \mathbf{u}(s) + [\hat{\Psi}(t, s) - \Psi(t, s)] \mathbf{R}_s \epsilon_\theta(\mathbf{u}(s), s), \quad (53)$$

which is the mean in Eq (20).

B.2.3 Proof of Theorem 1

We restate conclusion presented in Theorem 1. The exact solution $\mathbf{u}(t - \Delta t)$ to Eq (6) with coefficient Eq (8) is

$$\mathbf{u}(t - \Delta t) \sim \mathcal{N}\left(\sqrt{\frac{\alpha_{t-\Delta t}}{\alpha_t}}\mathbf{u}(t) + \left[-\sqrt{\frac{\alpha_{t-\Delta t}}{\alpha_t}}\sqrt{1-\alpha_t} + \sqrt{1-\alpha_{t-\Delta t}-\sigma_t^2}\right]\epsilon_\theta(\mathbf{u}(t), t), \sigma_t^2 \mathbf{I}_d\right) \quad (54)$$

with $\sigma_t^2 = (1 - \alpha_{t-\Delta t}) \left[1 - \left(\frac{1-\alpha_{t-\Delta t}}{1-\alpha_t}\right)^{\lambda^2} \left(\frac{\alpha_t}{\alpha_{t-\Delta t}}\right)^{\lambda^2}\right]$, which is the same as the DDIM Eq (9).

Theorem 1 is a concrete application of Eq (20) when the DM is a DDPM and $\mathbf{F}_\tau, \mathbf{G}_\tau$ are set to Eq (8). Thanks to the special form of \mathbf{F}_τ , Ψ has the expression

$$\Psi(t, s) = \sqrt{\frac{\alpha_t}{\alpha_s}} \mathbf{I}_d, \quad (55)$$

and $\hat{\Psi}$ satisfies

$$\log \hat{\Psi}(t, s) = \int_s^t \left[\frac{1}{2} \frac{d \log \alpha_\tau}{d\tau} - \frac{1 + \lambda^2}{2} \frac{d \log \alpha_\tau}{d\tau} \frac{1}{1 - \alpha_\tau} \right] d\tau \quad (56)$$

$$\hat{\Psi}(t, s) = \left(\frac{1 - \alpha_t}{1 - \alpha_s} \right)^{\frac{1+\lambda^2}{2}} \left(\frac{\alpha_s}{\alpha_t} \right)^{\frac{\lambda^2}{2}}. \quad (57)$$

Mean: Based on Eq (20), we obtain the mean of \hat{p}_{st} as

$$\sqrt{\frac{\alpha_t}{\alpha_s}}\mathbf{u}(s) + \left[-\sqrt{\frac{\alpha_t}{\alpha_s}}\sqrt{1-\alpha_s} + \left(\frac{1-\alpha_t}{1-\alpha_s} \right)^{\frac{1+\lambda^2}{2}} \left(\frac{\alpha_s}{\alpha_t} \right)^{\frac{\lambda^2}{2}} \sqrt{1-\alpha_s} \right] \epsilon_\theta(\mathbf{u}(s), s) \quad (58)$$

$$= \sqrt{\frac{\alpha_t}{\alpha_s}}\mathbf{u}(s) + \left[-\sqrt{\frac{\alpha_t}{\alpha_s}}\sqrt{1-\alpha_s} + \sqrt{(1-\alpha_t) \left(\frac{1-\alpha_{t-\Delta t}}{1-\alpha_t} \right)^{\lambda^2} \left(\frac{\alpha_t}{\alpha_{t-\Delta t}} \right)^{\lambda^2}} \right] \epsilon_\theta(\mathbf{u}(s), s) \quad (59)$$

$$= \sqrt{\frac{\alpha_t}{\alpha_s}}\mathbf{u}(s) + \left[-\sqrt{\frac{\alpha_t}{\alpha_s}}\sqrt{1-\alpha_s} + \sqrt{1-\alpha_t-\sigma_s^2} \right] \epsilon_\theta(\mathbf{u}(s), s), \quad (60)$$

where

$$\sigma_s^2 = (1 - \alpha_t) \left[1 - \left(\frac{1 - \alpha_t}{1 - \alpha_s} \right)^{\lambda^2} \left(\frac{\alpha_s}{\alpha_t} \right)^{\lambda^2} \right]. \quad (61)$$

Setting $(s, t) \leftarrow (t, t - \Delta t)$, we arrive at the mean update in Eq (13).

Covariance: It follows from

$$\frac{d\mathbf{P}_{s\tau}}{d\tau} = 2 \left[\frac{d \log \alpha_\tau}{2d\tau} - \frac{1 + \lambda^2}{2} \frac{d \log \alpha_\tau}{d\tau} \frac{1}{1 - \alpha_\tau} \right] \mathbf{P}_{s\tau} - \lambda^2 \frac{d \log \alpha_\tau}{d\tau} \mathbf{I}_d, \quad \mathbf{P}_{ss} = 0$$

that

$$\mathbf{P}_{st} = (1 - \alpha_t) \left[1 - \left(\frac{1 - \alpha_t}{1 - \alpha_s} \right)^{\lambda^2} \left(\frac{\alpha_s}{\alpha_t} \right)^{\lambda^2} \right].$$

Setting $(s, t) \leftarrow (t, t - \Delta t)$, we recover the covariance in Eq (13).

B.2.4 Proof of Prop 7

When $\lambda = 0$, the update step in Eq (20) from s to t reads

$$\mathbf{u}(t) = \Psi(t, s)\mathbf{u}(s) + [\hat{\Psi}(t, s) - \Psi(t, s)]\mathbf{R}_s \epsilon_\theta(\mathbf{u}(s), s). \quad (62)$$

Meanwhile, the update step in Eq (16) from s to t is

$$\mathbf{u}(t) = \Psi(t, s)\mathbf{u}(s) + \left[\int_s^t \frac{1}{2} \Psi(t, \tau) \mathbf{G}_\tau \mathbf{G}_\tau^T \mathbf{R}_\tau^{-T} d\tau \right] \epsilon_\theta(\mathbf{u}(s), s). \quad (63)$$

Eq (62) and (63) are equivalent once we have the following lemma.

Lemma 2. When $\lambda = 0$,

$$\int_s^t \frac{1}{2} \Psi(t, \tau) \mathbf{G}_\tau \mathbf{G}_\tau^T \mathbf{R}_\tau^{-T} d\tau = [\hat{\Psi}(t, s) - \Psi(t, s)] \mathbf{R}_s.$$

Proof. We introduce two new functions

$$\mathbf{N}(t) := \int_s^t \frac{1}{2} \Psi(t, \tau) \mathbf{G}_\tau \mathbf{G}_\tau^T \mathbf{R}_\tau^{-T} d\tau \quad (64)$$

$$\mathbf{M}(t) := [\hat{\Psi}(t, s) - \Psi(t, s)] \mathbf{R}_s. \quad (65)$$

First, $\mathbf{N}(s) = \mathbf{M}(s) = 0$. Second, they satisfy

$$\frac{d\mathbf{N}(t)}{dt} = \mathbf{F}_t \mathbf{N}(t) + \frac{1}{2} \mathbf{G}_t \mathbf{G}_t^T \mathbf{R}_t^{-T} \quad (66)$$

$$\frac{d\mathbf{M}(t)}{dt} = [\hat{\mathbf{F}}_t \hat{\Psi}(t, s) - \mathbf{F}_t \Psi(t, s)] \mathbf{R}_s \quad (67)$$

$$= \mathbf{F}_t \mathbf{M}(t) + \frac{1}{2} \mathbf{G}_t \mathbf{G}_t^T \Sigma_t^{-1} \hat{\Psi}(t, s) \mathbf{R}_s. \quad (68)$$

Note $\hat{\Psi}$ and \mathbf{R} satisfy the same linear differential equation as

$$\frac{d\hat{\Psi}(t, s)}{dt} = [\mathbf{F}_t + \frac{1}{2} \mathbf{G}_t \mathbf{G}_t^T \Sigma_t^{-1}] \hat{\Psi}(t, s), \quad \frac{d\mathbf{R}_t}{dt} = [\mathbf{F}_t + \frac{1}{2} \mathbf{G}_t \mathbf{G}_t^T \Sigma_t^{-1}] \mathbf{R}_t. \quad (69)$$

It is a standard result in linear system theory (see Särkkä & Solin [25, Eq(2.34)]) that $\hat{\Psi}(t, s) = \mathbf{R}_t \mathbf{R}_s^{-1}$. Plugging it and $\mathbf{R}_t \mathbf{R}_t^T = \Sigma_t$ into Eq (68) yields

$$\frac{d\mathbf{M}(t)}{dt} = \mathbf{F}_t \mathbf{M}(t) + \frac{1}{2} \mathbf{G}_t \mathbf{G}_t^T \mathbf{R}_t^{-T}. \quad (70)$$

Define $\mathbf{E}(t) = \mathbf{N}(t) - \mathbf{M}(t)$, then it satisfies

$$\mathbf{E}(s) = 0 \quad \frac{d\mathbf{E}(t)}{dt} = \mathbf{F}_t \mathbf{E}(t), \quad (71)$$

which clearly implies that $\mathbf{E}(t) = 0$. Thus, $\mathbf{N}(t) = \mathbf{M}(t)$. \square

C More experiment details

We present practical implementation of gDDIM and its application to CLD. We include training details for \mathbf{R}_t -based CLD proposed in this work and discuss necessary calculation overhead for executing gDDIM. More experiments are conducted to verify the effectiveness of gDDIM compared with other sampling algorithms. We report image sampling performance over average of 3 runs with different random seeds.

C.1 Training CLD

Our training pipeline, model architectures and hyperparameters are similar to those in Dockhorn et al. [5]. The main differences are in the choice of \mathbf{K}_t and loss weights $\mathbf{K}_t^{-1} \Lambda_t \mathbf{K}_t^{-T}$.

We change from $\mathbf{K}_t = \mathbf{L}_t$ to $\mathbf{K}_t = \mathbf{R}_t$. Unlike \mathbf{L}_t which has triangular structure and closed form expression, we rely on high accuracy numerical solver to solve \mathbf{R}_t . The triangular structure of \mathbf{L}_t and sparse pattern of \mathbf{G}_t for CLD in Eq (10) also have an impact on the training loss function of the score model. Due to special structure of \mathbf{G}_t , we only need to learn $\mathbf{s}_\theta(\mathbf{u}, t; \mathbf{v})$ signals present in the velocity channel. When $\mathbf{K}_t = \mathbf{L}_t$, $\mathbf{s}_\theta(\mathbf{u}, t) = -\mathbf{L}_t^{-T} \epsilon_\theta^{(\mathbf{L}_t)}(\mathbf{u}, t)$ with \mathbf{L}_t^{-T} being upper triangular. Thus we only need to train $\epsilon_\theta^{(\mathbf{L}_t)}(\mathbf{u}, t; \mathbf{v})$ to recover $\mathbf{s}_\theta(\mathbf{u}, t; \mathbf{v})$. In contrast, \mathbf{R}_t does not share the triangular structure as \mathbf{L}_t ; both $\epsilon_\theta^{(\mathbf{R}_t)}(\mathbf{u}, t; \mathbf{x})$, $\epsilon_\theta^{(\mathbf{R}_t)}(\mathbf{u}, t; \mathbf{v})$ are needed to recover $\mathbf{s}_\theta(\mathbf{u}, t; \mathbf{v})$. Therefore, Dockhorn et al. [5] sets loss weights

$$\mathbf{L}_t^{-1} \Lambda_t \mathbf{L}_t^{-T} = \begin{bmatrix} 0 & 0 \\ 0 & 1 \end{bmatrix} \otimes \mathbf{I}_d, \quad (72)$$

while we choose

$$\mathbf{R}_t^{-1} \Lambda_t \mathbf{R}_t^{-T} = \begin{bmatrix} 1 & 0 \\ 0 & 1 \end{bmatrix} \otimes \mathbf{I}_d. \quad (73)$$

As a result, we need to double the channel in the output layer in our new parameterization associated with \mathbf{R}_t , though the increased number of parameters in last layer is negligible compared with other parts of diffusion models.

We include the model architectures and hyperparameters in Tab 5. In addition to the standard size model on CIFAR10, we also train a smaller model for CELEBA to show the efficacy and advantages of gDDIM.

Table 5: Model architectures and hyperparameters

Hyperparameter	CIFAR10	CELEBA
Model		
EMA rate	0.9999	0.999
# of ResBlock per resolution	8	2
Normalization	Group Normalization	Group Normalization
Progressive input	Residual	None
Progressive combine	Sum	N/A
Finite Impluse Response	Enabled	Disabled
Embedding type	Fourier	Positional
# of arameters	$\approx 108\text{M}$	$\approx 62\text{M}$
Training		
# of iterations	1m	150k
Optimizer	Adam	Adam
Learning rate	2×10^{-4}	2×10^{-4}
Gradient norm clipping	1.0	1.0
Dropout	0.1	0.1
Batch size per GPU	32	32
GPUs	4 A6000	4 A6000
Trainig time	$\approx 78\text{h}$	$\approx 16\text{h}$

C.2 Calculation of constant coefficients

In gDDIM, many coefficients cannot be obtained in closed-form. Here we present our approach to obtain them numerically. Those constant coefficients can be divided into two categories, solutions to ODEs and definite integrals. We remark that these coefficients only need to be calculated once and then can be used everywhere. For CLD, each of these coefficient corresponds to a 2×2 matrix. The calculation of all these coefficients can be done within 1 min.

Type I: Solving ODEs The problem appears when we need to evaluate \mathbf{R}_t in Eq (15) and $\hat{\Psi}(t, s)$ in

$$\frac{d\hat{\Psi}(t, s)}{dt} = \hat{\mathbf{F}}_t \hat{\Psi}(t, s), \quad \hat{\Psi}(s, s) = \mathbf{I}. \quad (74)$$

Across our experiments, we use RK4 with a step size 10^{-6} to calculate the ODE solutions. For $\hat{\Psi}(t, s)$, we only need to calculate $\hat{\Psi}(t, 0)$ because $\hat{\Psi}(t, s) = \hat{\Psi}(t, 0)[\hat{\Psi}(s, 0)]^{-1}$. In CLD, $\mathbf{F}_t, \mathbf{G}_t, \mathbf{R}_t, \Sigma_t$ can be simplified to a 2×2 matrix; solving the ODE with a small step size is extremely fast. We note $\Psi(t, s)$ and Σ_t admit close-form formula [5]. Since the output of numerical solvers are discrete in time, we employ a linear interpolation to handle query in continuous time. Since $\mathbf{R}_t, \hat{\Psi}$ are determined by the forward SDE in DMs, the numerical results can be shared. In stochastic gDDIM Eq (20), we apply the same techniques to solve \mathbf{P}_{st} .

Type II: Definite integrals

The problem appears in the derivation of update step in Eq (16), (17b) and (42), which require coefficients such as ${}^p\mathbf{C}_{ij}^{(q)}, {}^c\mathbf{C}_{ij}^{(q)}$. We use step size 10^{-5} for the integration from t to $t - \Delta t$. The integrand can be efficiently evaluated in parallel using GPUs. Again, the coefficients, such as

		FID / IS at different NFE			
q	K_t	20	30	40	50
0	L_t	461.72 / 1.18	441.05 / 1.21	244.26 / 2.39	120.07 / 5.25
	R_t	17.94 / 8.47	9.84 / 9.00	6.87 / 9.19	5.46 / 9.31
1	L_t	368.38 / 1.32	232.39 / 2.43	99.45 / 4.92	57.06 / 6.70
	R_t	8.14 / 9.10	4.35 / 9.46	3.32 / 9.58	2.92 / 9.65
2	L_t	463.33 / 1.17	166.90 / 3.56	4.12 / 9.25	3.31 / 9.38
	R_t	4.54 / 9.42	2.66 / 9.64	2.39 / 9.74	2.32 / 9.75
3	L_t	464.36 / 1.17	463.45 / 1.17	463.32 / 1.17	240.45 / 2.29
	R_t	341.70 / 1.42	292.31 / 1.70	13.27 / 10.15	2.28 / 9.77

Table 6: More experiments on CIFAR10

$pC_{ij}^{(q)}, cC_{ij}^{(q)}$, are calculated once and used afterwards if we need sample another batch with the same time discretization.

C.3 More experiments on the choice of score parameterization

Here we present more experiments details and more experiments regarding [Prop 1](#) and differences between the two parameterizations involving R_t and L_t .

Toy experiments:

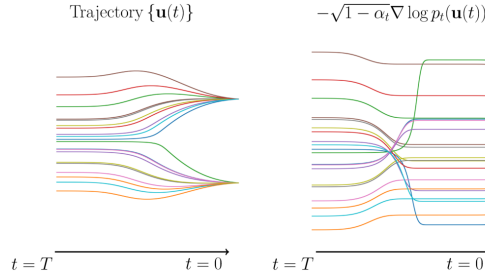


Figure 3: Trajectory and ϵ of Probability Flow solution in DDPM

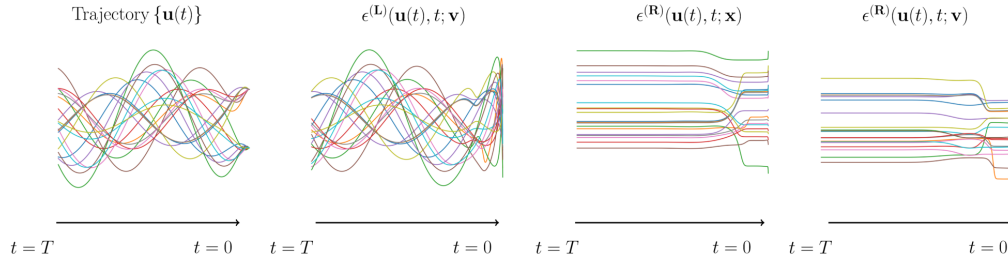


Figure 4: Trajectory and ϵ of Probability Flow solution in CLD

Here we present more empirical results to demonstrate the advantage of proper K_t .

In VPSDE, the advantage of DDIM has been verified in various models and datasets [28]. To empirically verify [Prop 1](#), we present one toy example where the data distribution is a mixture of two one dimension Gaussian distributions. In this toy example, the ground truth $\nabla \log p_t(\mathbf{u})$ is known. As it shown in [Fig 3](#), along the solution to probability flow ODE, the score parameterization $-R_t^T \log p_t(\mathbf{x})$ enjoys better smoothing property.

In CLD, we present a similar study. As the covariance in CLD is no longer diagonal, we find the difference of L_t parameterization and R_t parameterization is large in [Fig 4](#).

Image experiments:

q	K_t	FID at different NFE			
		20	30	40	50
0	L_t	446.56	430.59	434.79	379.73
	R_t	37.72	13.65	12.51	8.96
1	L_t	261.90	123.49	105.75	88.31
	R_t	12.68	7.78	5.93	5.11
2	L_t	446.74	277.28	6.18	5.48
	R_t	6.86	5.67	4.62	4.19
3	L_t	449.21	440.84	443.91	286.22
	R_t	386.14	349.48	20.14	3.85

Table 7: More experiments on CELEBA

We present more empirical results regarding the comparison between L_t and R_t . Note that we use exponential integrator for the parametrization L_t as well, similar to DEIS [42]. We vary the polynomial order q in multistep methods [42] and test sampling performance on CIFAR10 and CELEBA. In both datasets, we generate $50k$ images and calculate their FID. As shown in Tab 6 and 7, R_t has significant advantages, especially when NFE is small.

We also find that multistep method with a large q can harm sampling performance when NFE is small. This is reasonable; the method with larger q assumes the nonlinear function is smooth in a large domain and may rely on outdated information for approximation, which may worsen the accuracy.

C.4 More experiments on the choice of λ

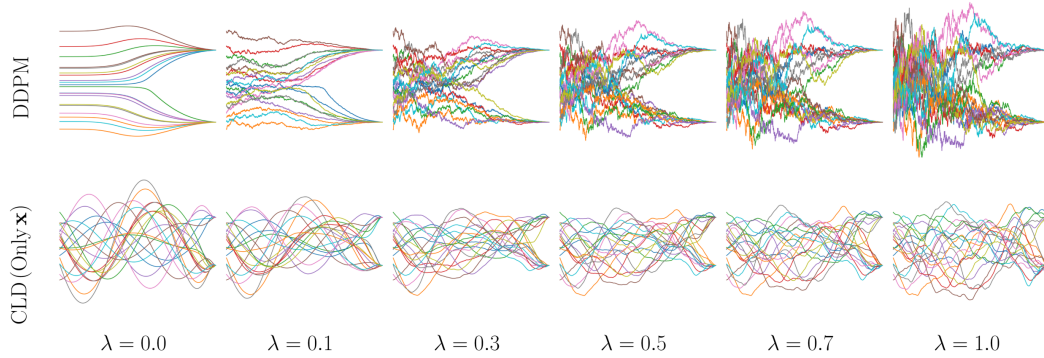


Figure 5: Sampling with various λ and accurate score on a Toy example. Trajectories are shown from T to 0.

To study the effects of λ , we visualize the trajectories generated with various λ but the same random seeds in Fig 5 on our toy example. Clearly, trajectories with smaller λ have better smoothing property while trajectories with large λ contain much more randomness. From the fast sampling perspective, trajectories with more stochasticity are much harder to predict with small NFE compared with smooth trajectories.

We include more qualitative results on the choice of λ and comparison between the Euler-Maruyama (EM) method and the gDDIM in Fig 8 and 9. Clearly, when NFE is small, increasing λ has a negative effect on the sampling quality of gDDIM. We hypothesize that $\lambda = 0$ already generates high-fidelity samples and additional noise may harm the sampling performance. With a fixed number of function evaluations, information derived from score network fails to remove the injected noise as we increase λ . On the other hand, we find that the EM method shows slightly better quality as we increase λ . We hypothesize that the ODE or SDEs with small λ has more oscillations than SDEs with large λ . It is known that the EM method has a very bad performance for oscillations systems and suffers from large discretization error [20]. From previous experiments, we find that ODE in CLD is highly oscillated.

We also find both methods perform worse than Symmetric Splitting CLD Sampler (SSCS) [5] when $\lambda = 1$. The improvement by utilizing Hamiltonian structure and SDEs structure is significant. This

encourages further exploration that incorporates Hamiltonian structure into gDDIM in the future. Nevertheless, we also remark that SSCS with $\lambda = 1.0$ performs much worse than gDDIM with $\lambda = 0$.

C.5 More comparisons

We also compare the performance of the CLD model we trained with that claimed in Dockhorn et al. [5] in Tab 8. We find that our trained model performs worse than Dockhorn et al. [5] when a blackbox ODE solver or EM sampling scheme with large NFE are used. There may be two reasons. First, with similar size model, our training scheme not only needs to fit $\nabla_v \log p_t(\mathbf{u})$, but also $\nabla_x \log p_t(\mathbf{u})$, while Dockhorn et al. [5] can allocate all representation resources of neural network to $\nabla_v \log p_t(\mathbf{u})$. Another factor is the mixed score trick on parameterization, which is shown empirically have a boost in model performance [5] but we do not include it in our training.

We also compare our algorithm with more accelerating sampling methods in Tab 8. gDDIM has achieved the best sampling acceleration results among training-free methods, but it still cannot compete with some distillation-based acceleration methods.

Table 8: More comparison on CIFAR10

Class	Model	NFE (\downarrow)	FID (\downarrow)
CLD	our CLD-SGM (gDDIM)	50	2.28
	our CLD-SGM (SDE, EM)	2000	2.43
	our CLD-SGM (Prob.Flow, RK45)	157	3.16
	CLD-SGM (Prob.Flow, RK45) by Dockhorn et al. [5]	147	2.71
	CLD-SGM (SDE, EM) by Dockhorn et al. [5]	2000	2.23
Training-free Accelerated Score	DDIM by Song et al. [28]	100	4.16
	Gotta Go Fast by Jolicœur-Martineau et al. [9]	151	2.73
	Analytic-DPM by Bao et al. [3]	100	3.55
	FastDPM by Kong & Ping [12]	100	2.86
	PNDM by Liu et al. [14]	100	3.53
	DEIS by Zhang & Chen [42]	50	2.99
Training-needed Accelerated Score	DDSS by Watson et al. [38]	25	4.25
	Progressive Distillation by Salimans & Ho [24]	4	3.0
	Knowledge distillation by Luhman & Luhman [15]	1	9.36

C.6 Code licenses

We implemented gDDIM and related algorithms in Jax. We have used code from a number of sources in Tab 9.

URL	Citation	License
https://github.com/yang-song/score_sde	[31]	Apache License 2.0
https://github.com/nv-tlabs/CLD-SGM	[5]	NVIDIA Source Code License
https://github.com/qsh-zh/deis	[42]	Unknown

Table 9: Code License

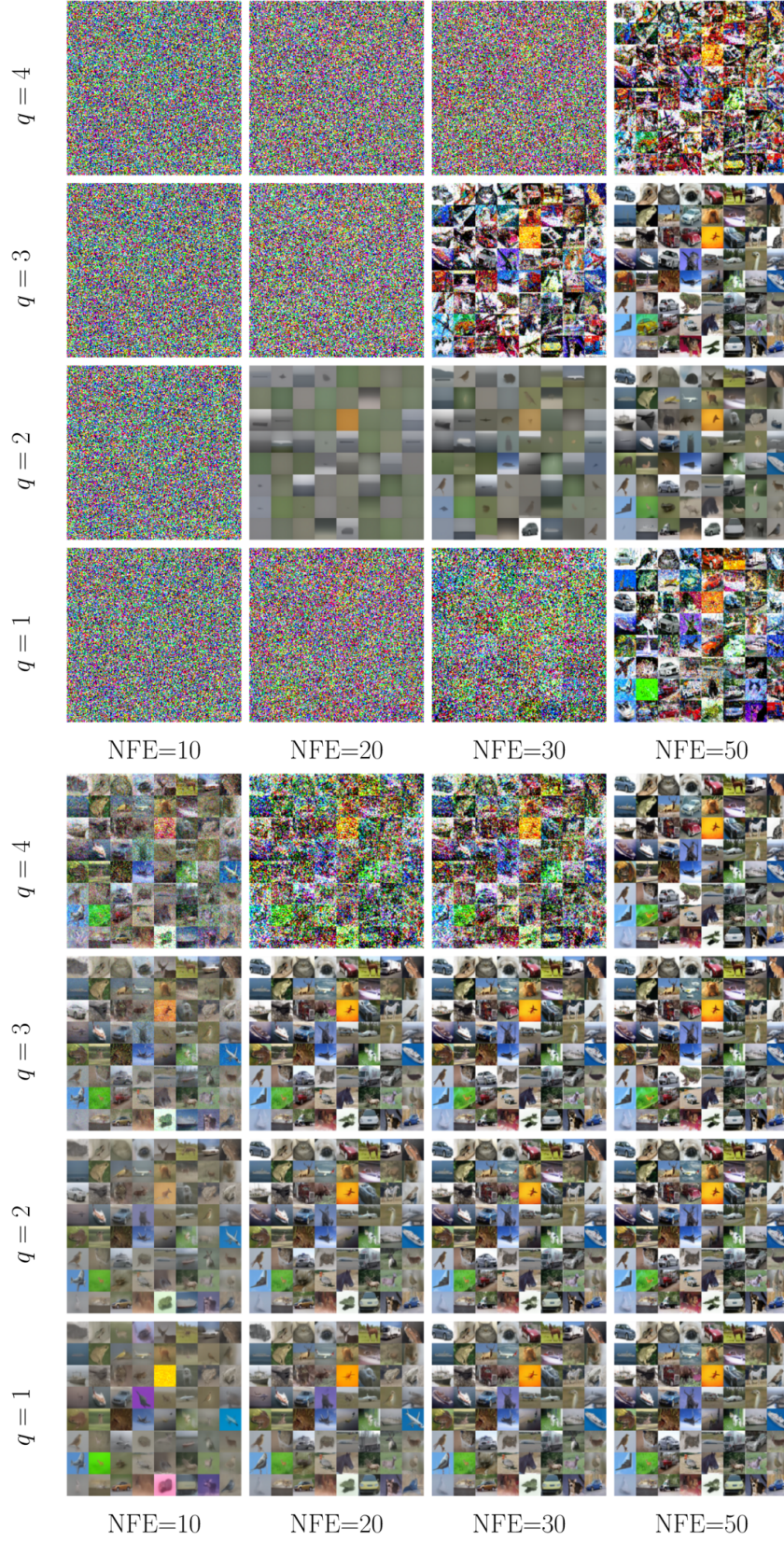


Figure 6: Comparison between L (Upper) and R (Lower) with exponential integrator on CIFAR10.

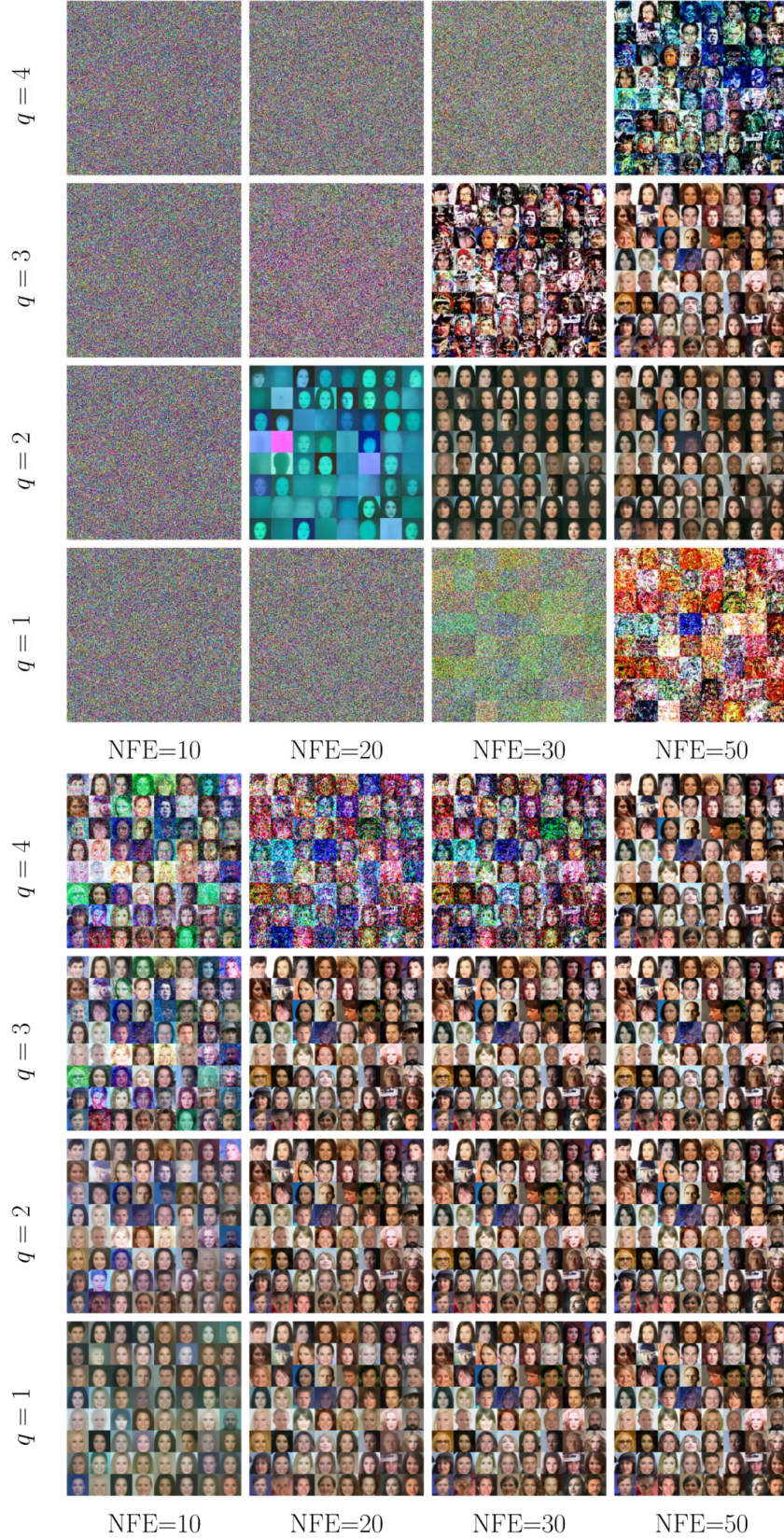


Figure 7: Comparison between L (Upper) and R (Lower) with exponential integrator on CELEBA.

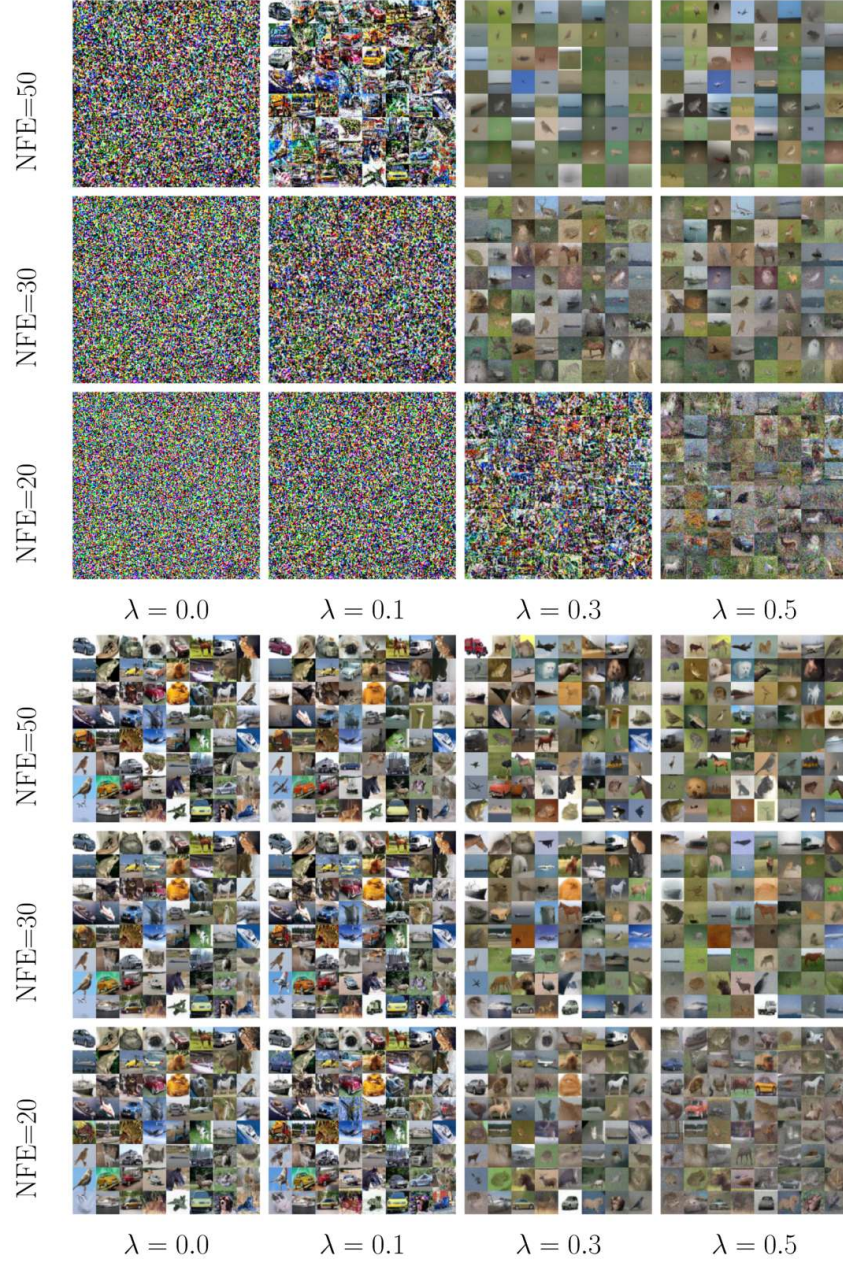


Figure 8: Comparison between EM (Upper) and gDDIM (Lower) on CIFAR10.

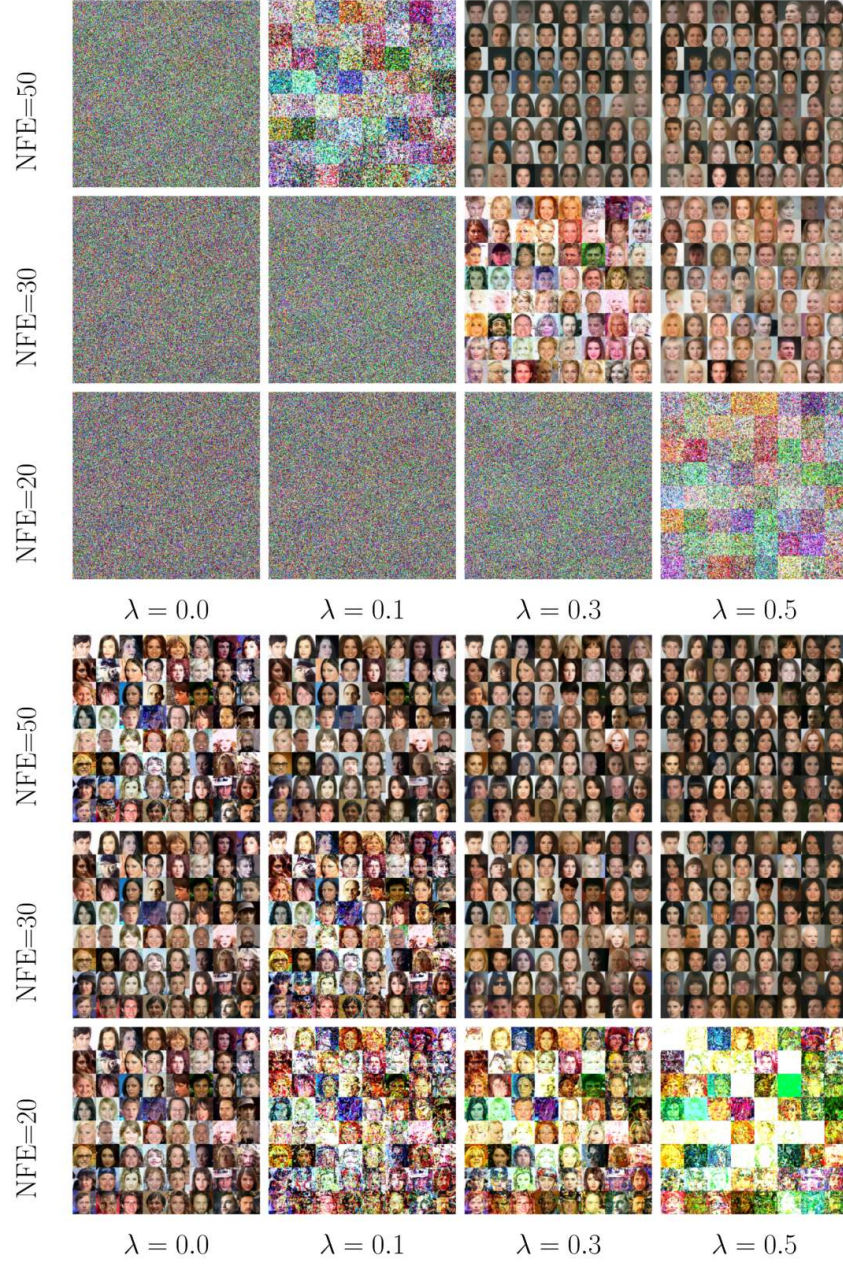


Figure 9: Comparison between EM (Upper) and gDDIM (Lower) on CELEBA.